# Variogram Inversion and Uncertainty Using Dynamic Data

Z. A. Reza (zreza@ualberta.ca) and C. V. Deutsch (cdeutsch@civil.ualberta.ca)
Department of Civil & Environmental Engineering, University of Alberta

X. H. Wen (xwen@chevrontexaco.com)
ChevronTexaco Exploration and Production Technology Company

## Abstract

*Data paucity is a major obstacle for variography in reservoir characterization. With only a few well data, it is hardly possible to model reasonably good horizontal variograms. Expert modeler would take recourse of experience or analogue information to get around this simple yet important very important aspect of reservoir modeling. The outcome of such a recourse can often lead to disastrous petrophysical models; the situation often blamed as a handicap of geostatistics. Here is a technique developed to address the problem by using information available from production history or well test data.*

*The technique developed here builds upon a dynamic data integration technique for generating permeability, porosity models. An automatic variogram fitting module is incorporated into this algorithm to dynamically update the variogram models. The initial result of this approach is remarkably positive. A measurable amount of reduction in variography uncertainty is possible through this approach. This has been demonstrated through some synthetic and realistic examples.*

## Simultaneouos Inversion with Variogram Updating

There are rarely enough data to calculate reliable variograms. This is particularly true in petroleum reservoir characterization. It is hardly possible to model reasonably good horizontal variograms with a few well data. Expert modeler would use experience or analogue information; however, each reservoir is unique and the reasonableness of analogue data can always be questioned. In this chapter, we present a technique to assist with variogram inference by using information available from production history or well test data. The new algorithm further improves upon the inversion solutions that are obtained using the algorithm presented in [1].

The algorithm will be explained. We demonstrate the results of the developed code with some synthetic realistic reservoir models. The outcome of this approach in addressing the problem is remarkable when sufficient production data exist.

## Variogram Inversion Algorithm

The algorithm developed here builds upon the algorithm presented in [1]. We extend this dynamic data integration algorithm for petrophysical property modeling to invert for spatial continuity parameters. In order to achieve this, we have implemented a module to determine updated experimental variograms of the property models, and another module to automatically fit these dynamically updated experimental variograms. The automatic variogram fitting module relies on an 'almost' exhaustive search algorithm in a $L^2$ norm basis. The $L^2$ norm is calculated using an inverse squared distance weighting approach where short distances are emphasized.

The inversion code requires additional parameters for variogram inversion. One needs the parameters required for experimental variogram calculation. Namely, the number of lags, lag distance, lag tolerance, azimuth angles, angle tolerance and bandwidths.

### Extension for Variogram Updating

The incorporation of experimental variogram calculation and automatic variogram modeling module is as follows:

1. Perform Steps (1) to (10) discussed for simultaneous inversion algorithm in [1] using a priori variogram information.
2. Calculate experimental variograms of updated $\phi$ and $\ln(k)$ fields.
3. Perform automatic variogram modeling with an 'almost' exhaustive search algorithm based on a weighted $L^2$ norm.
4. Update the prior variogram parameters with the new ones.
5. Repeat Steps (1) to (4) until convergence is achieved in the inversion process.

In this modified algorithm the variogram models that are to be used for kriging at each outer iteration are updated. This updating is naturally informed to some extent by the production data at each outer iteration. In the original version of the algorithm, the variogram models are kept unchanged. Thus, even if incremental information is captured from production data, the initial variogram information of is used at each outer iteration. The new algorithm removes some of these restictions by dynamically updating the variogram models. The parameters that are fitted in the updating module are the ranges of each variogram structure, sill contribution, angle of anistropy, and nugget effect.

## A Synthetic Application

A synthetic example is presented here to evaluate the ability of the algorithm to invert for variogram parameters using multiple well production data. Reference porosity and permeability models are constructed first. Pressure responses at a number of wells are obtained through flow simulation.

The 2D 4,000-ft square domain is discretized into $40 \times 40$ grid cells of $100 \times 100$ ft. Porosity and permeability fields are shown in Figure 1. There are four wells: W1 at the center of the cell (24,10), W2 at (37,17), W3 at (14,32), and W4 at (35,31). Wells are shown in Figure 1. The four boundaries are constant pressure boundaries, reservoir thickness is 100 ft, viscosity is 0.2 cp, formation compressibility is $10^{-6}$ psi$^{-1}$, and well radius is 0.3 ft. Figure 2 shows the imposed production rates and the corresponding numerically simulated pressure responses at the different wells. The global histograms and the scatter-plot between porosity and $\ln(k)$ are shown in Figures 3 and 4, respectively. Mean and standard deviation of reference distributions are 0.13 and 0.06 for $\phi$, and 1.43 and 1.96 for $\ln(k)$. The low average porosity confirms the low storativity of the reservoir. Correlation coefficient of the two distributions is 0.79. Variogram for both $\phi$ and $\ln(k)$ of the reference fields are shown in Figure 5. The well data is inadequate for variogram inference. Using only this many data, one can hardly model or infer horizontal variograms. Even with unusually large lag tolerance and bandwidth used in variogram estimation, realistic variograms could not be estimated (shown in Figure 6). We do not have much confidence in the variograms estimated from the well data. Our objective here is to account for production data and estimate a realistic variogram model for the reservoir.

The data integration algorithm devised here requires the well data, the production history (or well test data), global distribution information and a prior guess of the variogram model. We employ the reference distributions as the global distribution information. It is true that we do not have this information a priori; we could use an approximate global distribution informed by some secondary data (for instance, seismic data). Static well used in the example are shown in Figure 7.

In order to demonstrate the ability of the developed code for variogram estimation and uncertainty, we use a number of prior variogram models and analyze the updated variograms in each of the runs.

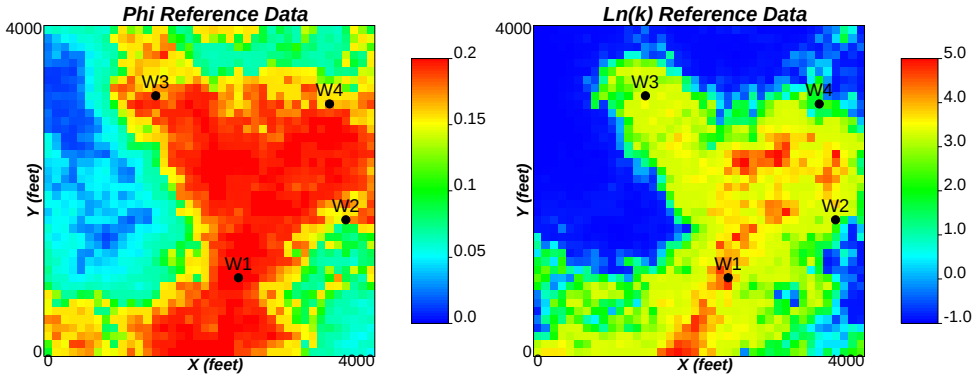


Figure 1: Reference $\phi$ and $\ln(k)$ fields: Example 1.

| **V. No.** | **Type** | **Sill** | **Range** X - Y (ft) | **Angle** ($^o$) |
|---|---|---|---|---|
| 0 | Nugget | 0.0 | | |
| 1 | Sph | 0.141 | 1000 - 9720 | 0 |
| 2 | Sph | 0.859 | 1475 - 1135 | 0 |

Table 1: Final variogram model obtained for $\phi$ after 15 iterations: Example 1 Run 1.

## Run 1

The prior variogram models used in this run for $\phi$ and $\ln(k)$ are given in Equations 1 and 2:

$$\gamma_\phi(h) = 0.05 + 0.5Sph(h)\begin{matrix} a_x = 7000 \\ a_y = 7000 \end{matrix} + 0.45Sph(h)\begin{matrix} a_x = 4000 \\ a_y = 4000 \end{matrix} \tag{1}$$

and

$$\gamma_y(h) = 0.05 + 0.55Sph(h)\begin{matrix} a_x = 3500 \\ a_y = 3500 \end{matrix} + 0.4Sph(h)\begin{matrix} a_x = 6000 \\ a_y = 6000 \end{matrix} . \tag{2}$$

The data integration code was run for 15 outer iterations using $6 \times 6$ (=36) master points in each iteration. CPU time for the run was only 320 seconds in a 1.8 GHz Pentium 4 personal computer. The updated variograms for $\phi$ and $\ln(k)$ are shown in Figures 8, 9, 10, and 11, for directions with azimuth 0 and 90. A close look at the variograms indicates improvement of the estimated variograms with the iterations. The dynamic data integration mismatch in $L^2$ norms for each iteration is shown in Figure 12. The final $L^2$ norm of the pressure march was 6.51. The prior initial variogram models were isotropic for both $\phi$ and $\ln(k)$, however the estimated variograms at each iteration reveals a reasonable anisotropy. It should be pointed that with inverse squared distance mismatch norm for variogram updating, it is difficult to good match at large lag distances in the updated model. The reason being the higher weights given to short lag distances. After 15 iterations, the final updated variogram models are given in Tables 1 and 2, respectively for $\phi$ and $\ln(k)$. It is evident that this approach can provide a more realistic variogram than what we get from the experimental variogram (Figure 6) using only static well data.

## Run 2

The prior variogram models used in this run for $\phi$ and $\ln(k)$ are given in Equations 3 and 4:

$$\gamma_\phi(h) = 0.25 + 0.5Sph(h)\begin{matrix} a_x = 1000 \\ a_y = 1000 \end{matrix} + 0.25Sph(h)\begin{matrix} a_x = 4000 \\ a_y = 4000 \end{matrix} \tag{3}$$

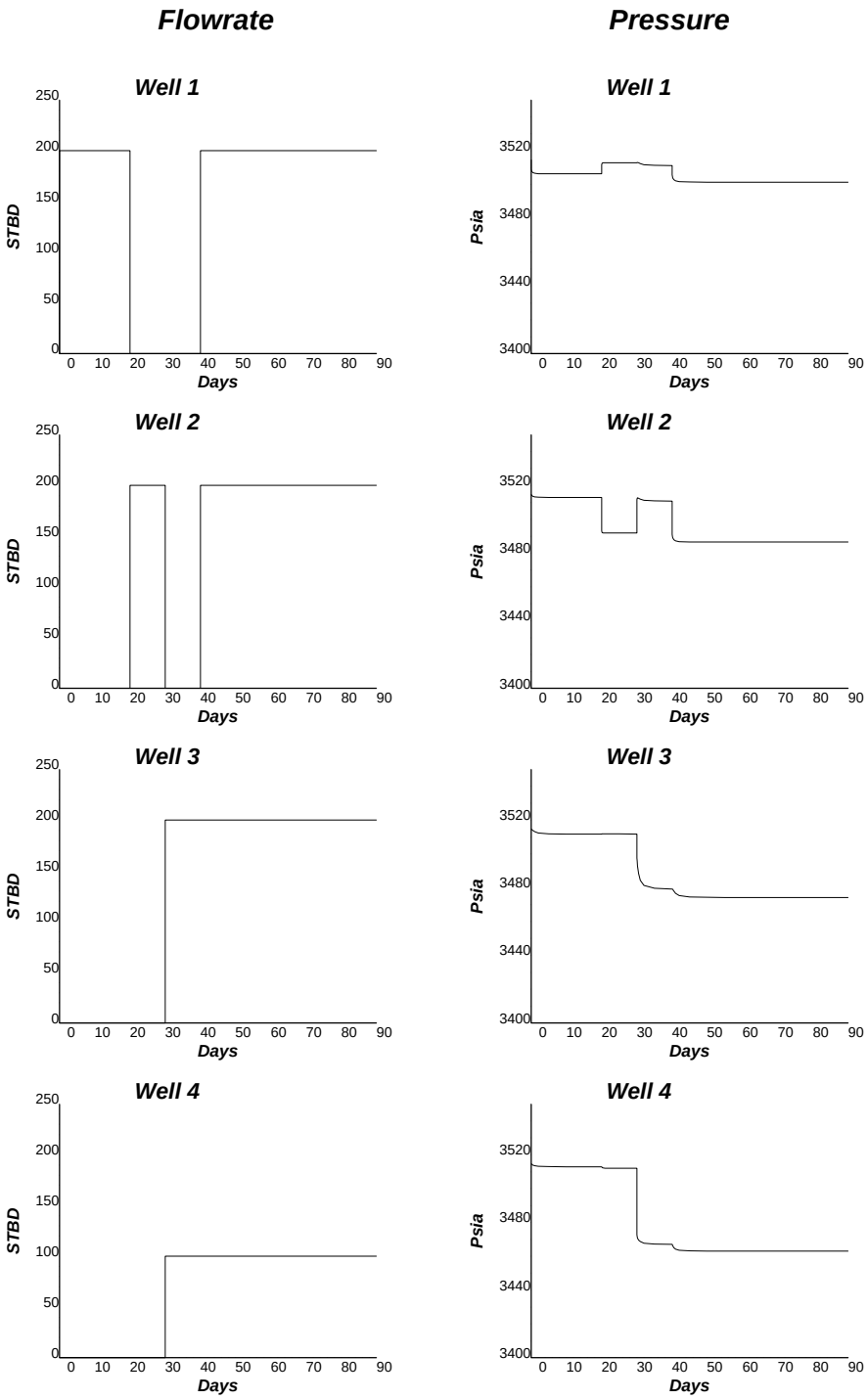


Figure 2: Production data (pressure and flow rates) obtained from the reference field: Example 1.

| **V. No.** | **Type** | **Sill** | **Range** X - Y (ft) | **Angle** ($^o$) |
|---|---|---|---|---|
| 0 | Nugget | 0.008 | | |
| 1 | Sph | 0.482 | 1425 - 1062 | 0 |
| 2 | Sph | 0.51 | 1600 - 1184 | 0 |

Table 2: Final variogram model obtained for $\ln(k)$ after 15 iterations: Example 1 Run 1.

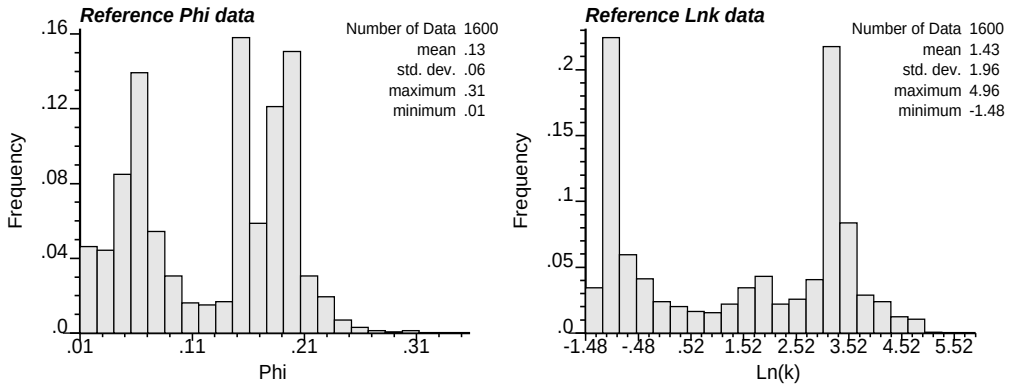


Figure 3: Histograms of reference $\phi$ and $\ln(k)$ fields: Example 1.

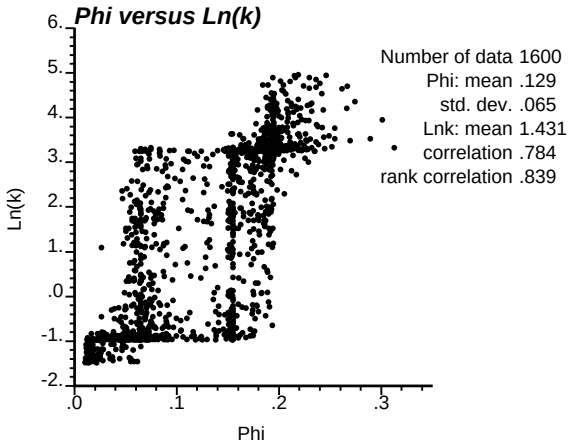


Figure 4: Scatterplot between reference $\phi$ and $\ln(k)$ values: Example 1.

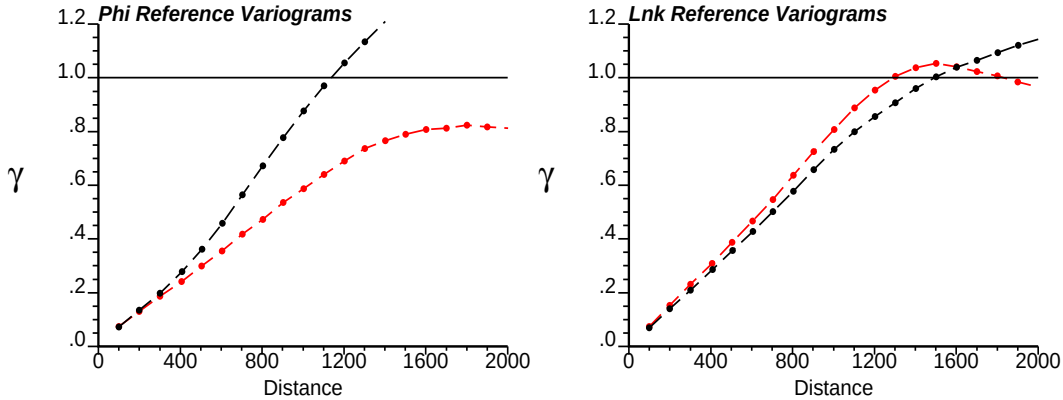


Figure 5: Variograms of reference $\phi$ and $\ln(k)$ distributions: Example 1. (X direction - dark, Y direction - light)

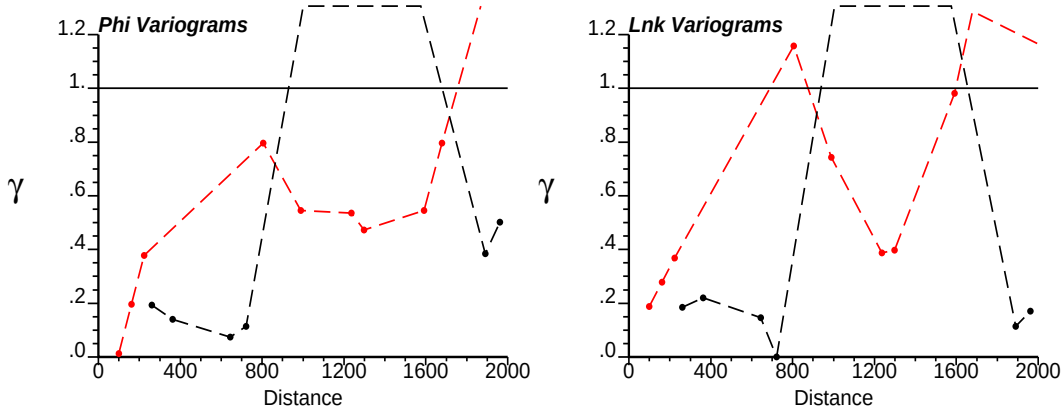


Figure 6: Variograms estimated from well data for $\phi$ and $\ln(k)$: Example 1. (X direction - dark, Y direction - light)

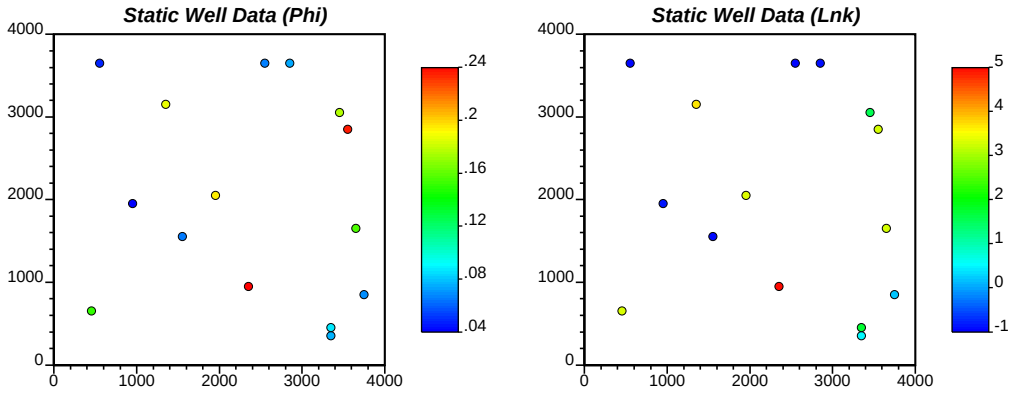


Figure 7: Static well data for $\phi$ and $\ln(k)$: Example 1.

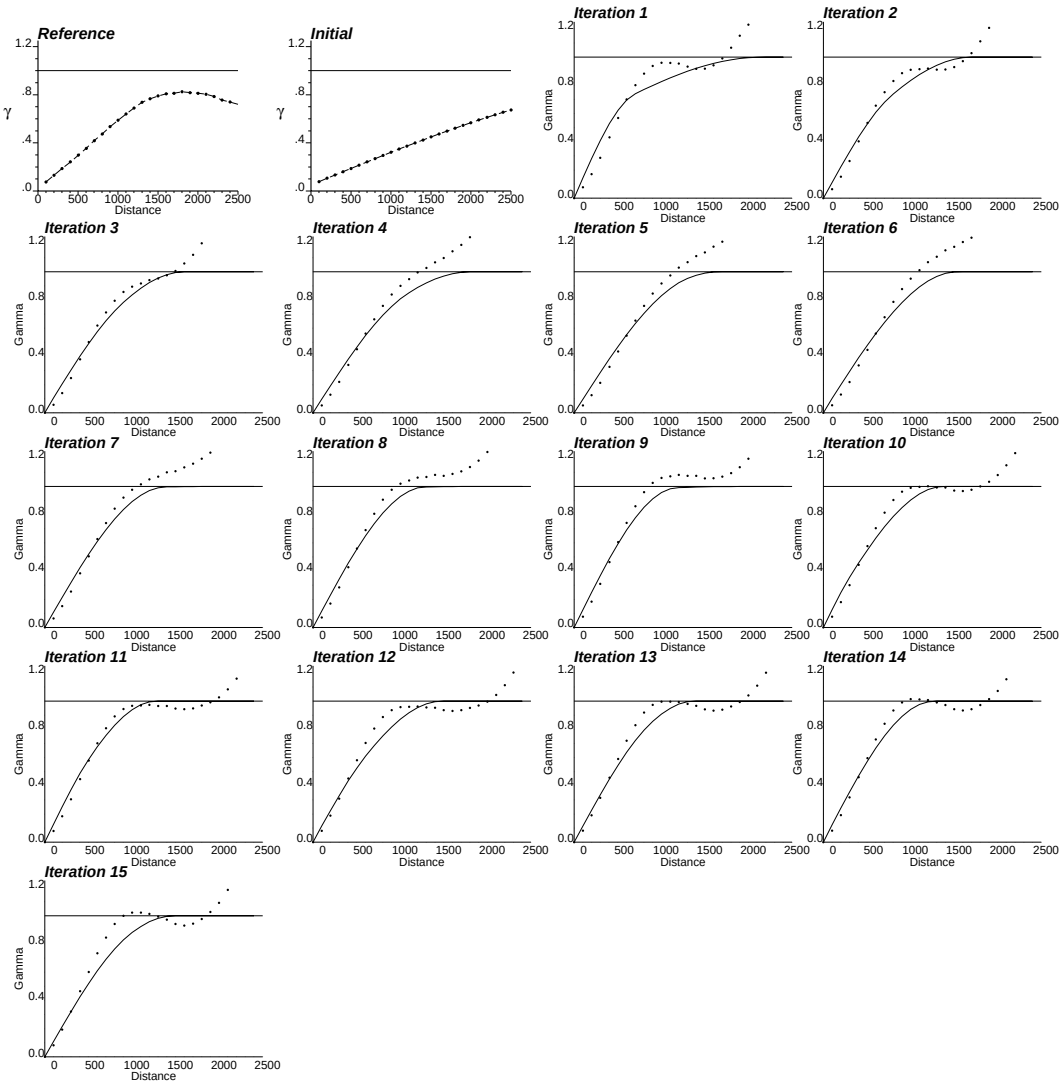


Figure 8: Reference, prior and updated variograms (experimental - dotted line, model - solid line) for $\phi$ at each outer iteration: Example 1 Run 1. (Direction with azimuth 0)

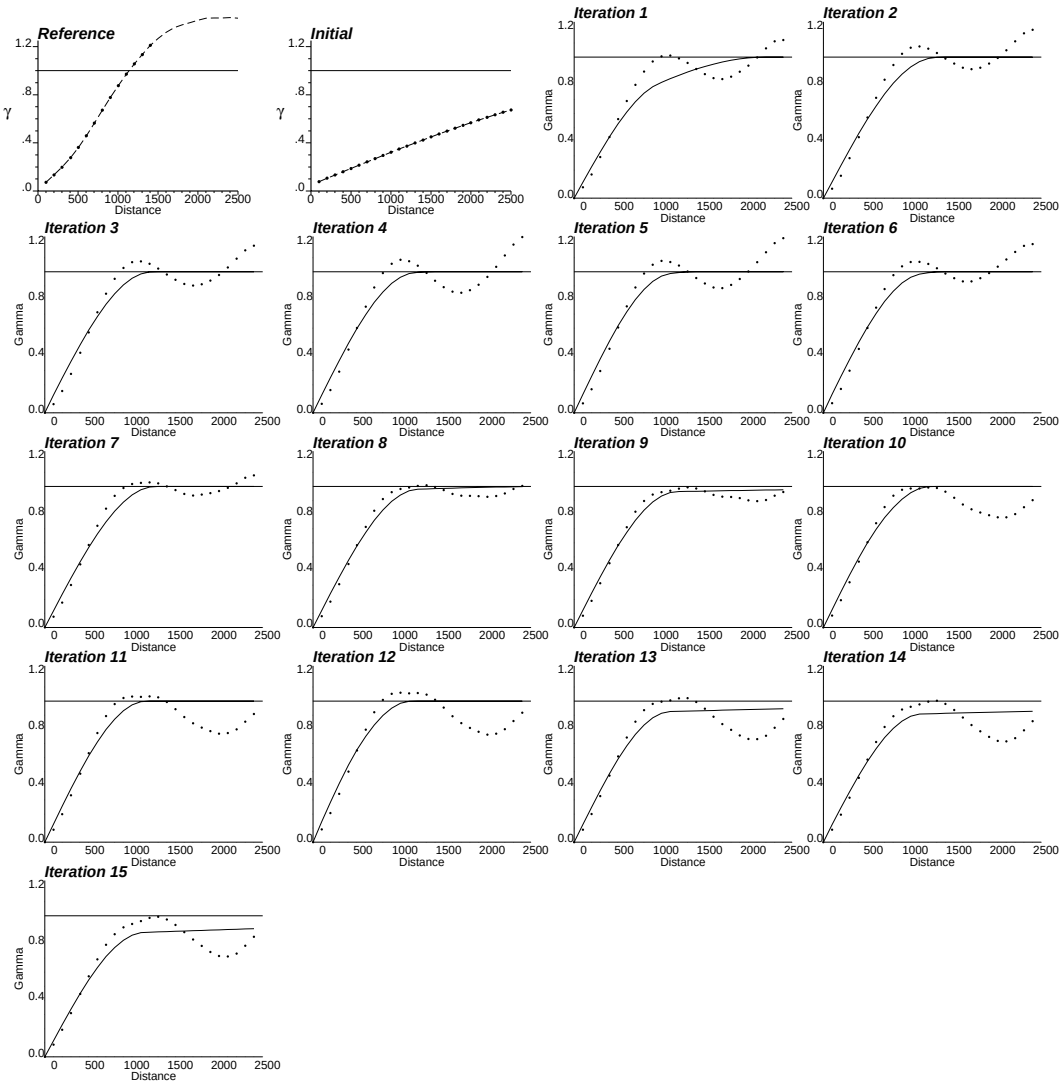


Figure 9: Reference, prior and updated variograms (experimental - dotted line, model - solid line) for $\phi$ at each outer iteration: Example 1 Run 1. (Direction with azimuth 90)

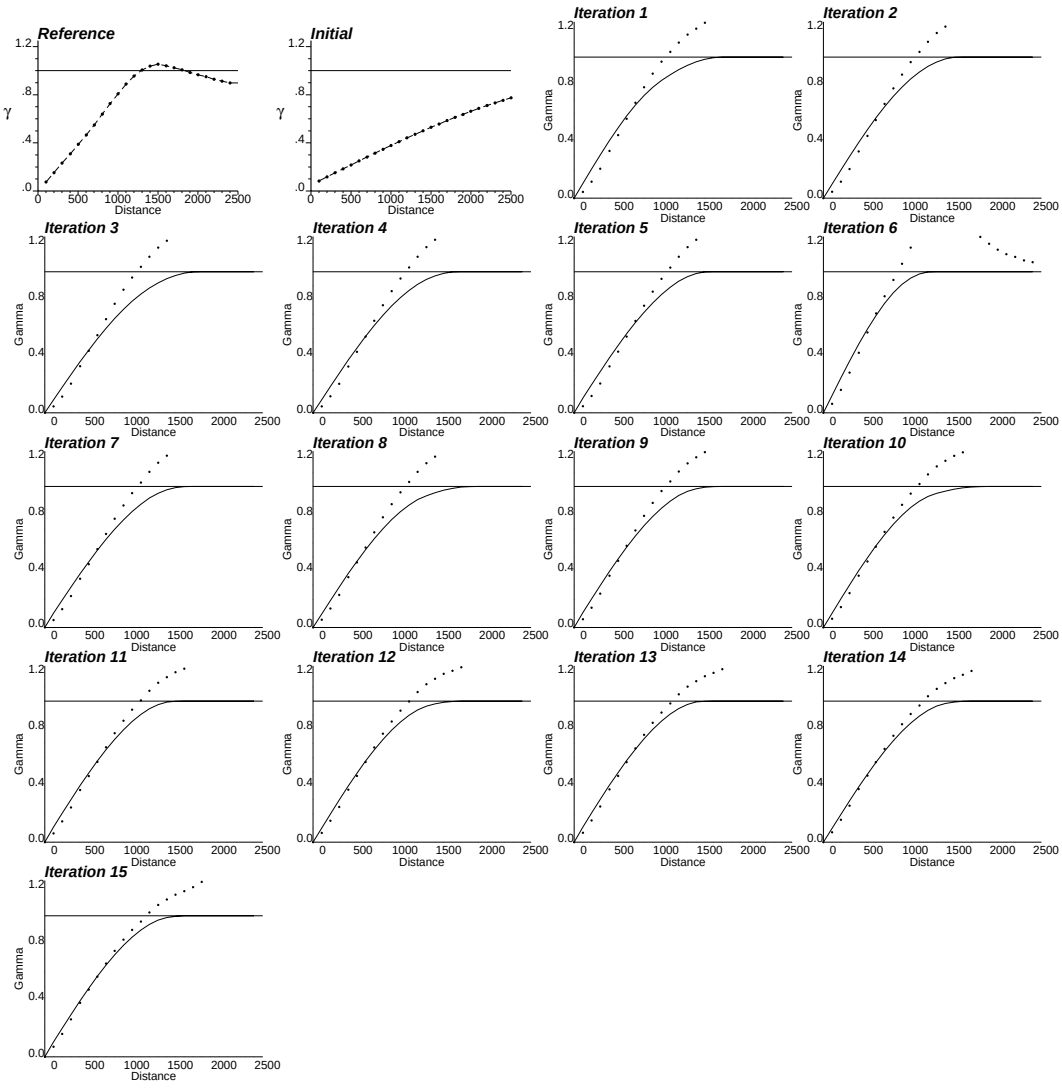


Figure 10: Reference, prior and updated variograms (experimental - dotted line, model - solid line) for $\ln(k)$ at each outer iteration: Example 1 Run 1. (Direction with azimuth 0)

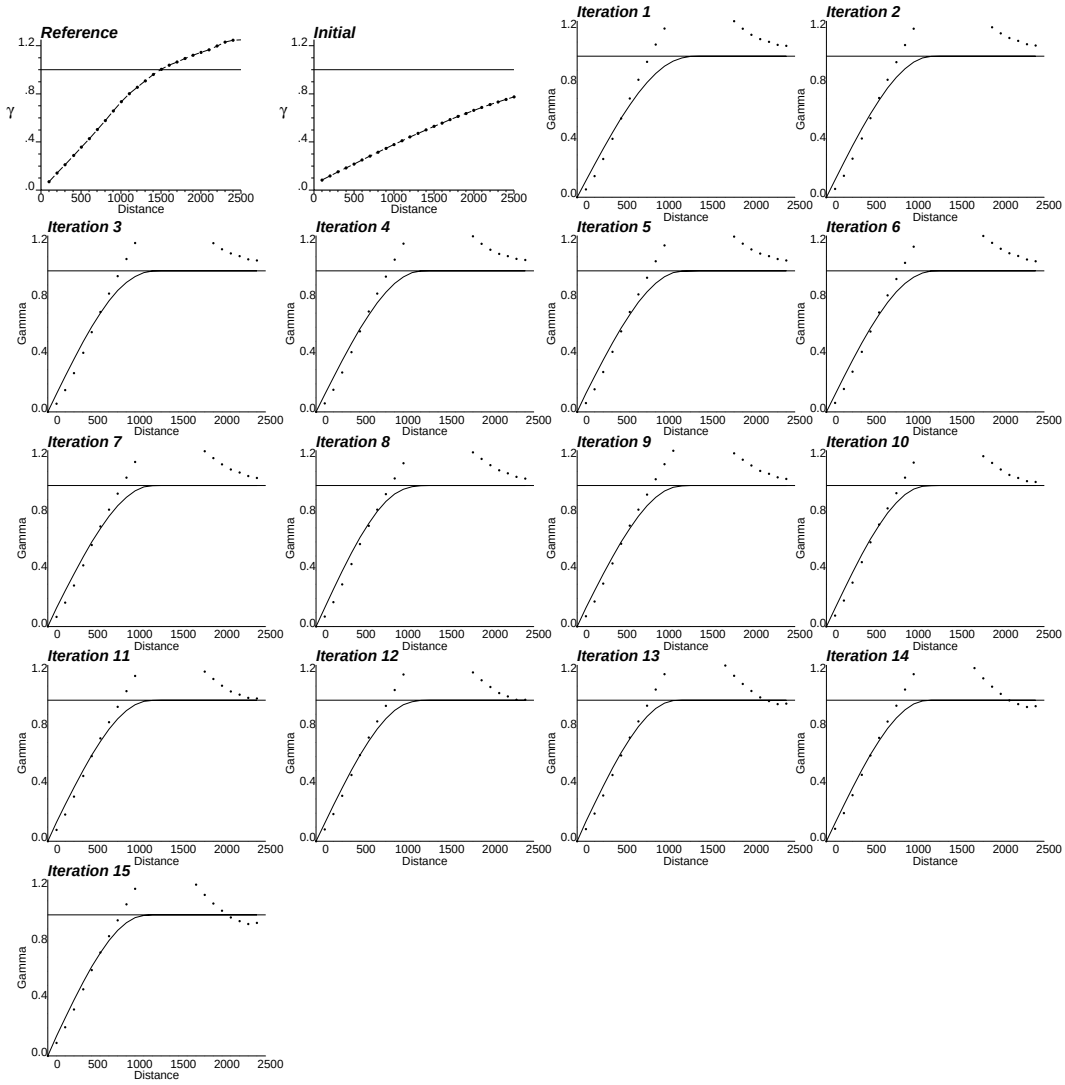


Figure 11: Reference, prior and updated variograms (experimental - dotted line, model - solid line) for $\ln(k)$ at each outer iteration: Example 1 Run 1. (Direction with azimuth 90)

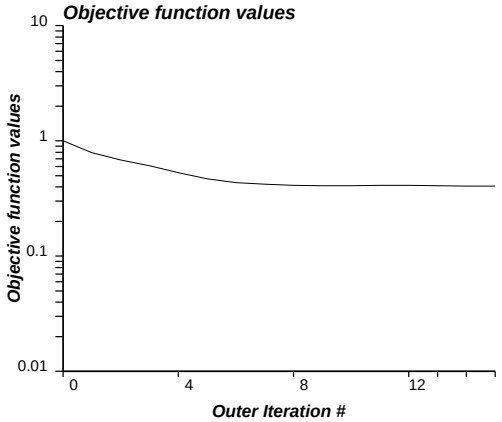


Figure 12: Mismatch norm of data integration at each outer iteration: Example 1 Run 1.

| V. No. | Type | Sill | Range X - Y (ft) | Angle ($^o$) |
|---|---|---|---|---|
| 0 | Nugget | 0.047 | | |
| 1 | Sph | 0.176 | 1050 - 911 | 0 |
| 2 | Sph | 0.777 | 1062 - 861 | 0 |

Table 3: Final variogram model obtained for $\phi$ after 15 iterations: Example 1 Run 2.

| V. No. | Type | Sill | Range X - Y (ft) | Angle ($^o$) |
|---|---|---|---|---|
| 0 | Nugget | 0.001 | | |
| 1 | Sph | 0.058 | 800 - 420 | 0 |
| 2 | Sph | 0.941 | 1312 - 1100 | 0 |

Table 4: Final variogram model obtained for $\ln(k)$ after 15 iterations: Example 1 Run 2.

and

$$\gamma_y(h) = 0.25 + 0.55Sph(h)\begin{matrix} a_x = 1500 \\ a_y = 1500 \end{matrix} + 0.2Sph(h)\begin{matrix} a_x = 6000 \\ a_y = 6000 \end{matrix}. \quad (4)$$

The nugget effect in the prior variograms is increased and the ranges are decreased for both $\phi$ and $\ln(k)$ compared to those used in Run 1. The data integration code was run for 15 outer iterations using $6 \times 6$ (=36) master points in each iteration. CPU time for the run was only 295 seconds in a 1.8 GHz Pentium 4 personal computer. The updated variograms for $\phi$ and $\ln(k)$ are shown in Figures 13, 14, 15, and 16, for directions with azimuth 0 and 90. A close look at the variograms indicates improvement of the estimated variograms with the iterations. The dynamic data integration mismatch in $L^2$ norms for each iteration is shown in Figure 17. The final $L^2$ norm of the pressure march was 6.04. The prior initial variogram models were isotropic for both $\phi$ and $\ln(k)$, however the estimated variograms at each iteration reveals a reasonable anisotropy. After 15 outer iterations, the final updated variogram models are given in Tables 3 and 4, respectively for $\phi$ and $\ln(k)$. It is evident that this approach can provide a more realistic variogram than what we get from the experimental variogram (Figure 6) obtained using only static well data. The prior variogram models had a nugget effect of 0.25 that was updated to almost negligible nugget effect which is closer to the reference.

## Run 3

The prior variogram models used in this run for $\phi$ and $\ln(k)$ are given in Equations 5 and 6:

$$\gamma_\phi(h) = 0.75 + 0.05Sph(h)\begin{matrix} a_x = 1000 \\ a_y = 1000 \end{matrix} + 0.2Sph(h)\begin{matrix} a_x = 7000 \\ a_y = 7000 \end{matrix} \quad (5)$$

and

$$\gamma_y(h) = 0.75 + 0.05Sph(h)\begin{matrix} a_x = 1500 \\ a_y = 1500 \end{matrix} + 0.2Sph(h)\begin{matrix} a_x = 8000 \\ a_y = 8000 \end{matrix}. \quad (6)$$

The nugget effect in the prior variograms is increased to 75% for both $\phi$ and $\ln(k)$ in this case. The data integration code was run for 16 outer iterations using $6 \times 6$ (=36) master points in each iteration. CPU time for the run was only 312 seconds in a 1.8 GHz Pentium 4 personal computer. The updated variograms for $\phi$ and $\ln(k)$ are shown in Figures 18, 19, 20, and 21, for directions with azimuth 0 and 90. A close look at the variograms indicates improvement of the estimated variograms with the iterations. The dynamic data integration mismatch in $L^2$ norms for each iteration is shown in Figure 22. The final $L^2$ norm of the pressure march was 0.588, a remarkably low mismatch value. The prior initial variogram models were isotropic for both $\phi$ and $\ln(k)$, however the estimated variograms at each iteration reveals a reasonable anisotropy. After 16 outer iterations, the final updated variogram models are given in Tables 5 and 6 for $\phi$ and $\ln(k)$. It is evident that this approach can provide a more realistic variogram than what we get from the experimental variogram

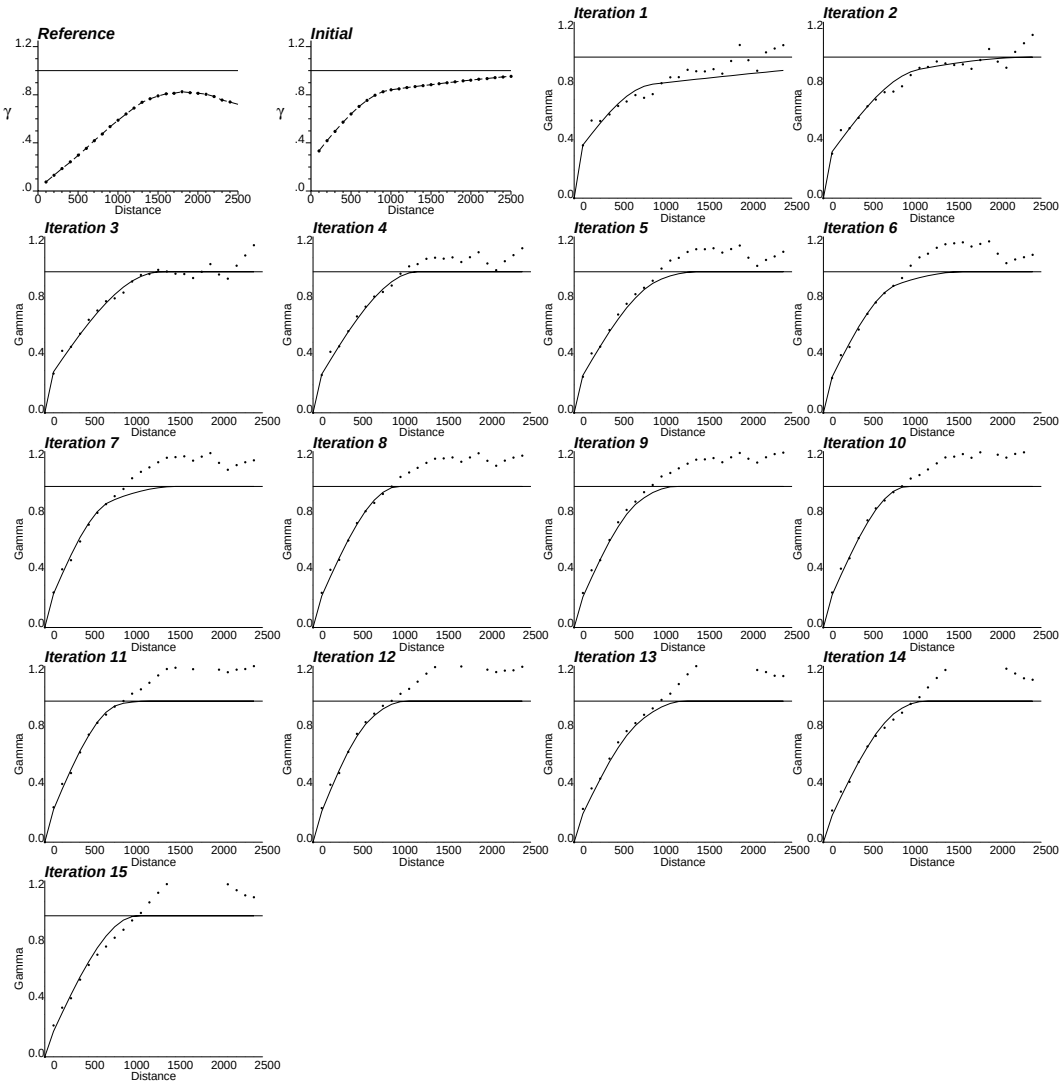


Figure 13: Reference, prior and updated variograms (experimental - dotted line, model - solid line) for $\phi$ at each outer iteration: Example 1 Run 2. (Direction with azimuth 0)

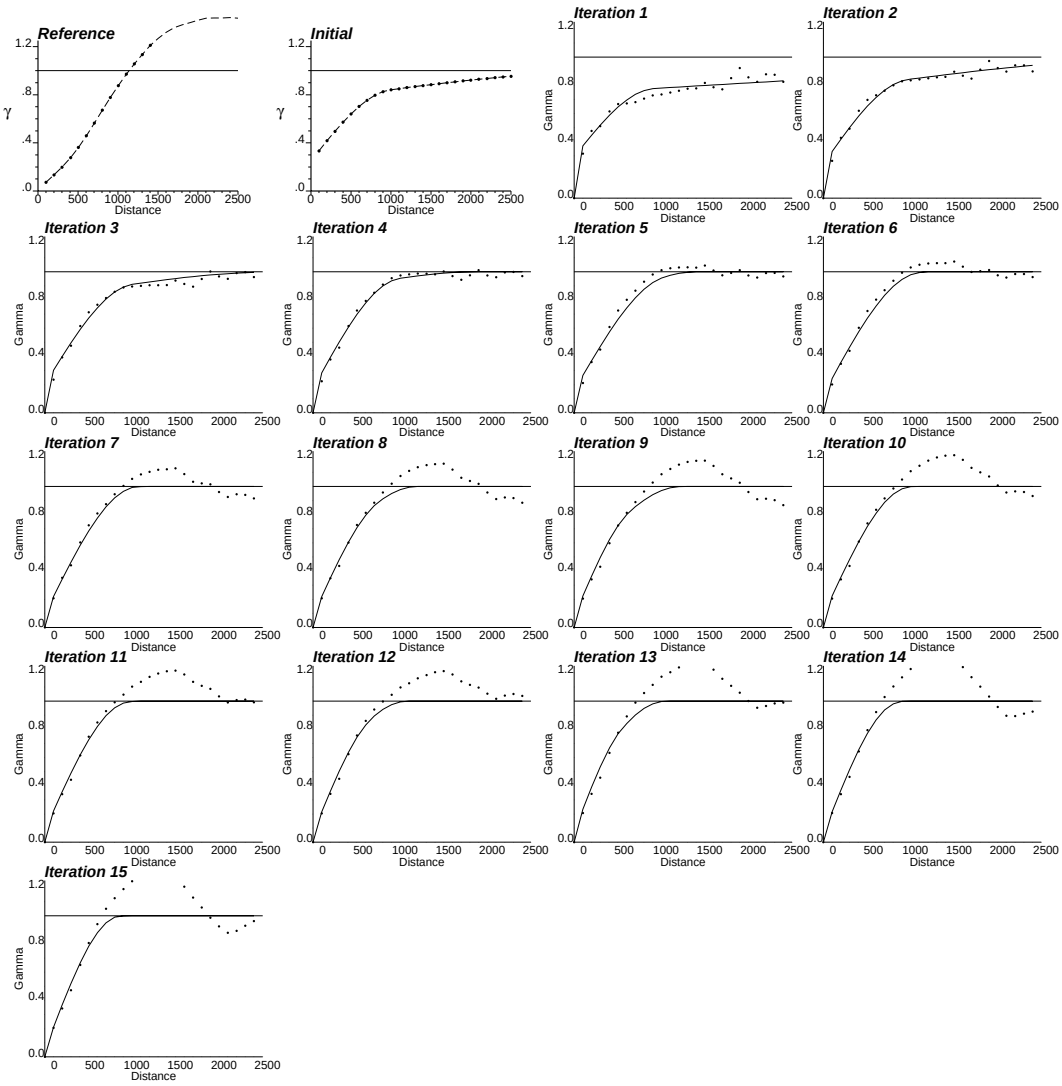


Figure 14: Reference, prior and updated variograms (experimental - dotted line, model - solid line) for $\phi$ at each outer iteration: Example 1 Run 2. (Direction with azimuth 90)

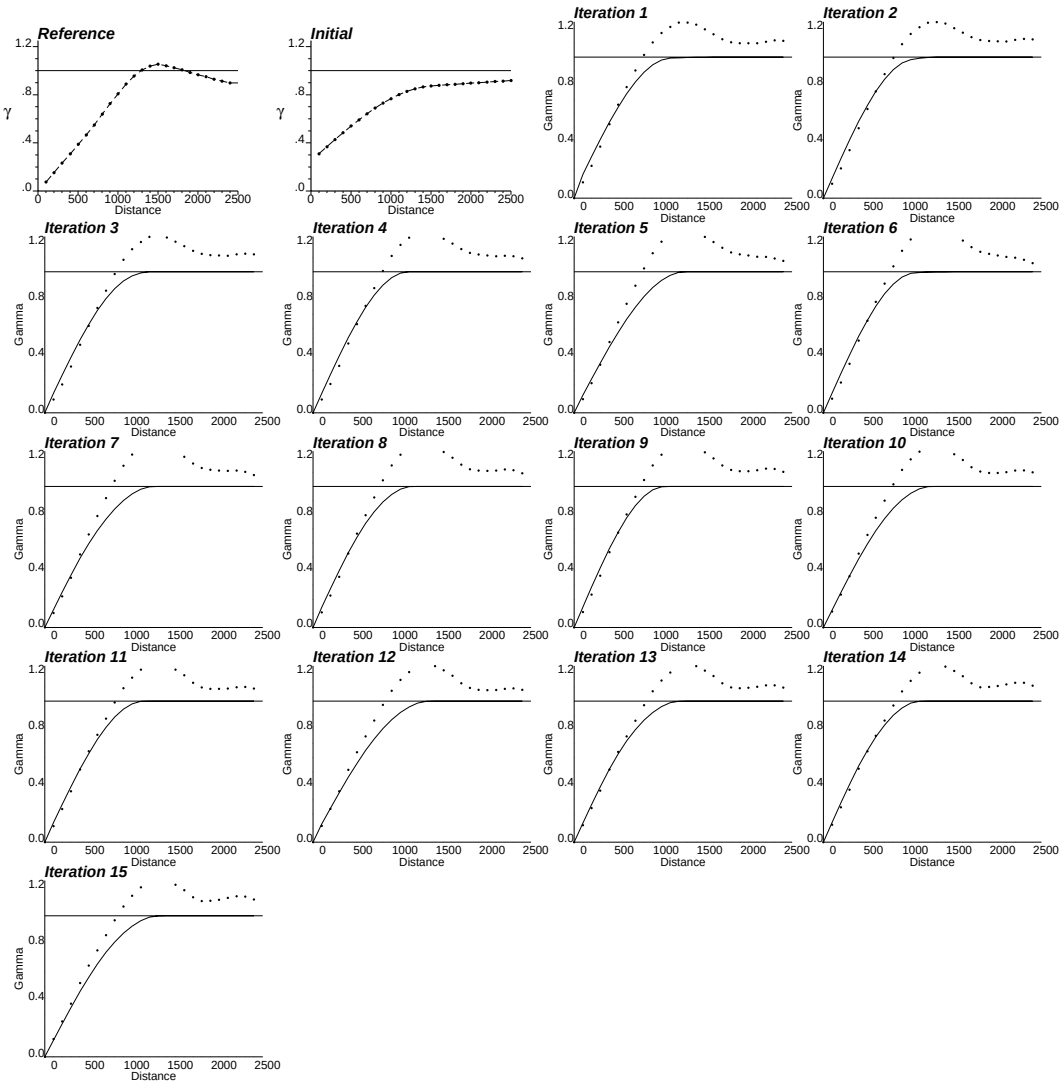


Figure 15: Reference, prior and updated variograms (experimental - dotted line, model - solid line) for $\ln(k)$ at each outer iteration: Example 1 Run 2. (Direction with azimuth 0)

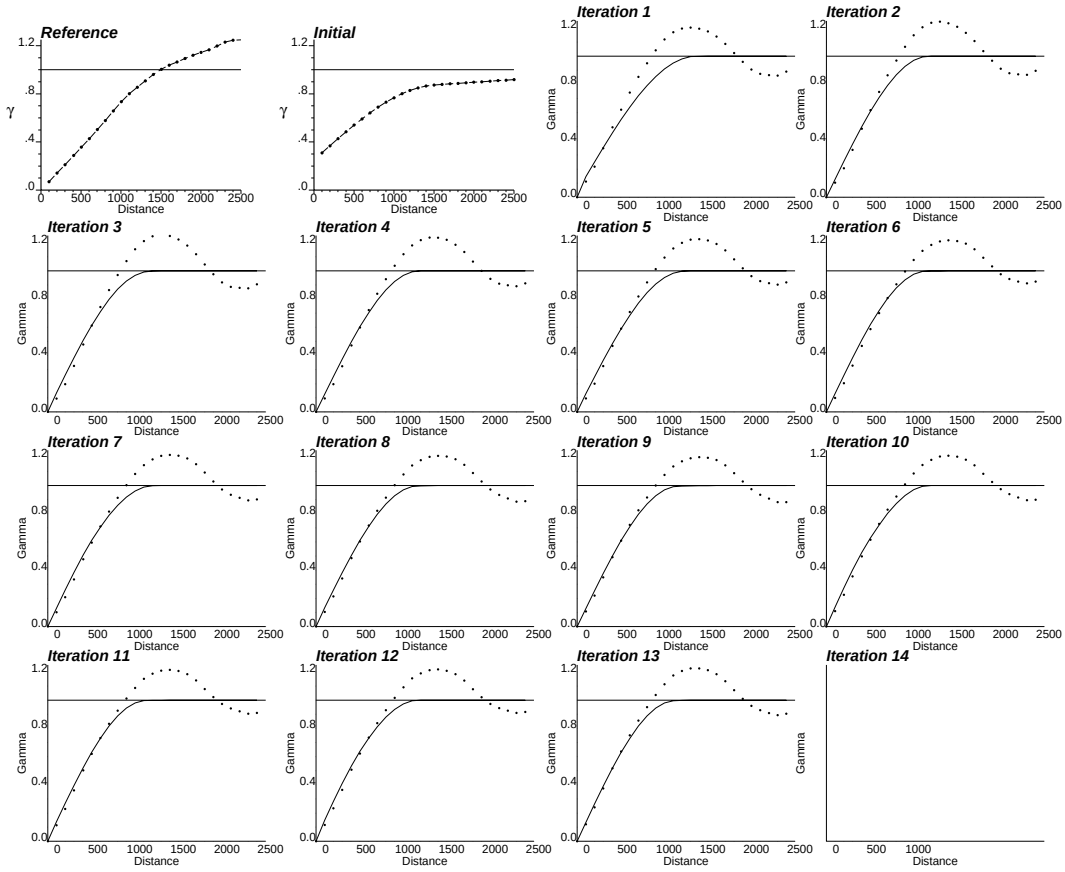


Figure 16: Reference, prior and updated variograms (experimental - dotted line, model - solid line) for $\ln(k)$ at each outer iteration: Example 1 Run 2. (Direction with azimuth 90)

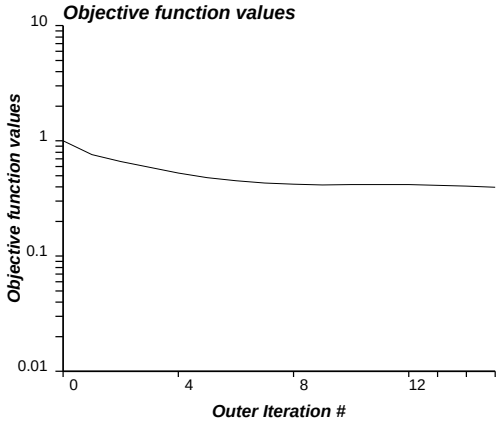


Figure 17: Mismatch norm of data integration at each outer iteration: Example 1 Run 2.

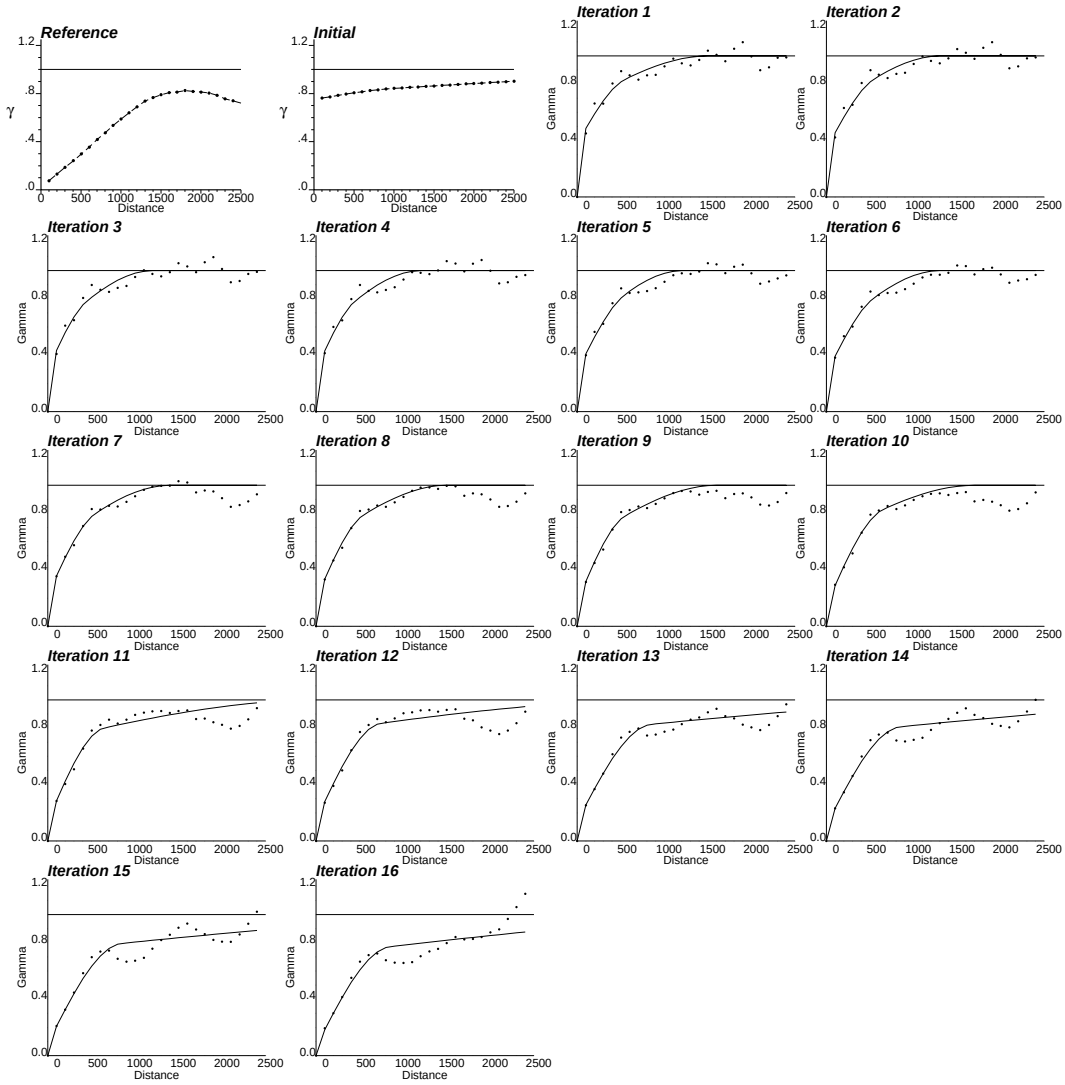


Figure 18: Reference, prior and updated variograms (experimental - dotted line, model - solid line) for $\phi$ at each outer iteration: Example 1 Run 3. (Direction with azimuth 0)

(Figure 6). The prior variogram model with high nugget effect of 0.75 led to final updated variogram model with a low nugget effect close to the reference value.

## Some Conclusions From Example One

Having analyzed the updated variograms in the first example, it could be concluded that the developed code provides reasonably good variogram models using multiple well production data. Some of the salient features of variogram information extraction from production data in this example are the following.

- Irrespective of prior variogram models with high or low nugget effect, we get back the low nugget effect of the reference distribution. It should be noted that the experimental variograms are obtained from gridded distribution, thus the smallest lag distance depends on the smallest dimension of the grid blocks.
- Range convergence is good for both $\phi$ and $\ln(k)$.

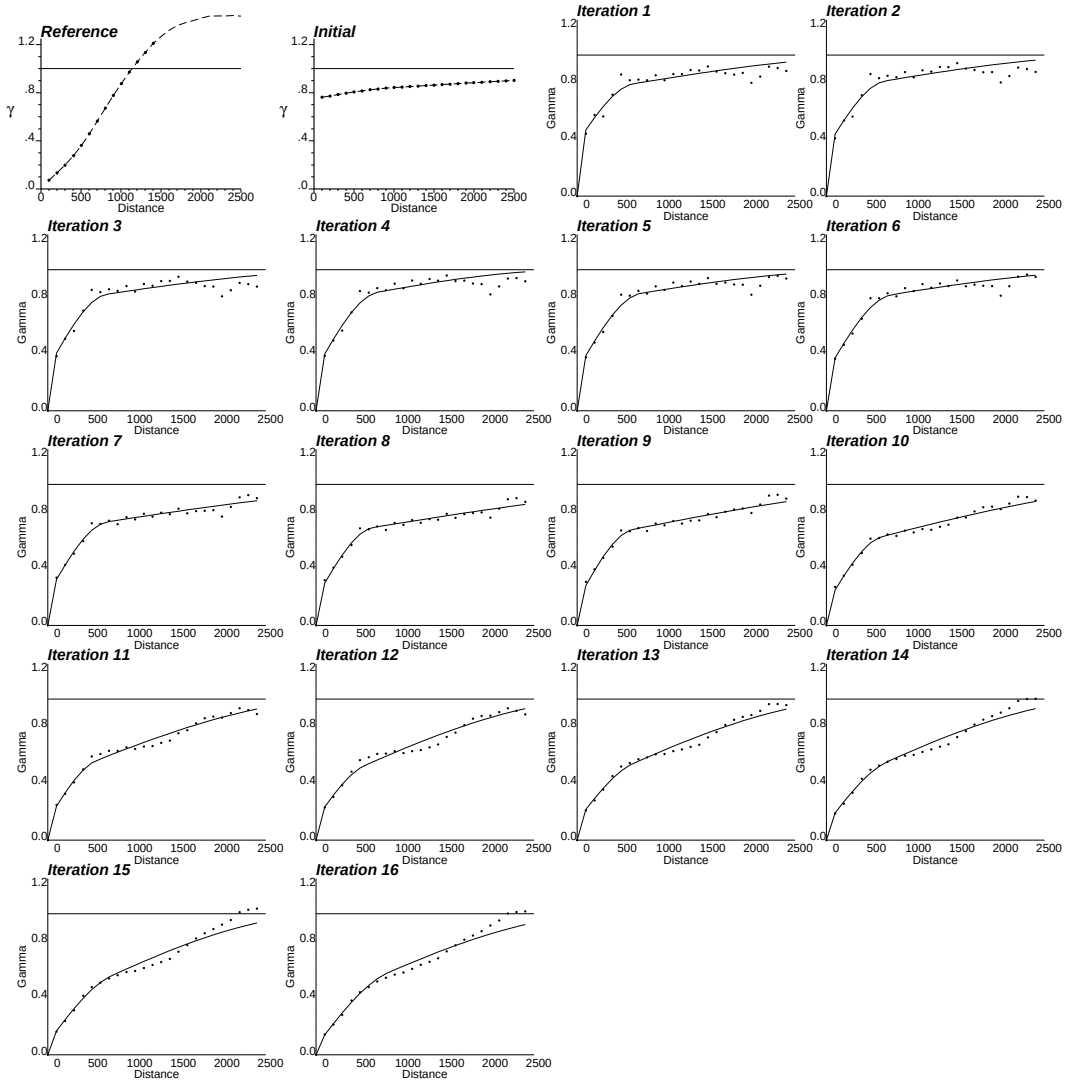


Figure 19: Reference, prior and updated variograms (experimental - dotted line, model - solid line) for $\phi$ at each outer iteration: Example 1 Run 3. (Direction with azimuth 90)

| **V. No.** | **Type** | **Sill** | **Range** X - Y (ft) | **Angle** ($^o$) |
|---|---|---|---|---|
| 0 | Nugget | 0.063 | | |
| 1 | Sph | 0.649 | 850 - 3404 | 0 |
| 2 | Sph | 0.288 | 5937 - 831 | 0 |

Table 5: Final variogram model obtained for $\phi$ after 16 iterations: Example 1 Run 3.

| **V. No.** | **Type** | **Sill** | **Range** X - Y (ft) | **Angle** ($^o$) |
|---|---|---|---|---|
| 0 | Nugget | 0.072 | | |
| 1 | Sph | 0.053 | 1312 - 220 | 0 |
| 2 | Sph | 0.875 | 1400 - 2310 | 0 |

Table 6: Final variogram model obtained for $\ln(k)$ after 16 iterations: Example 1 Run 3.

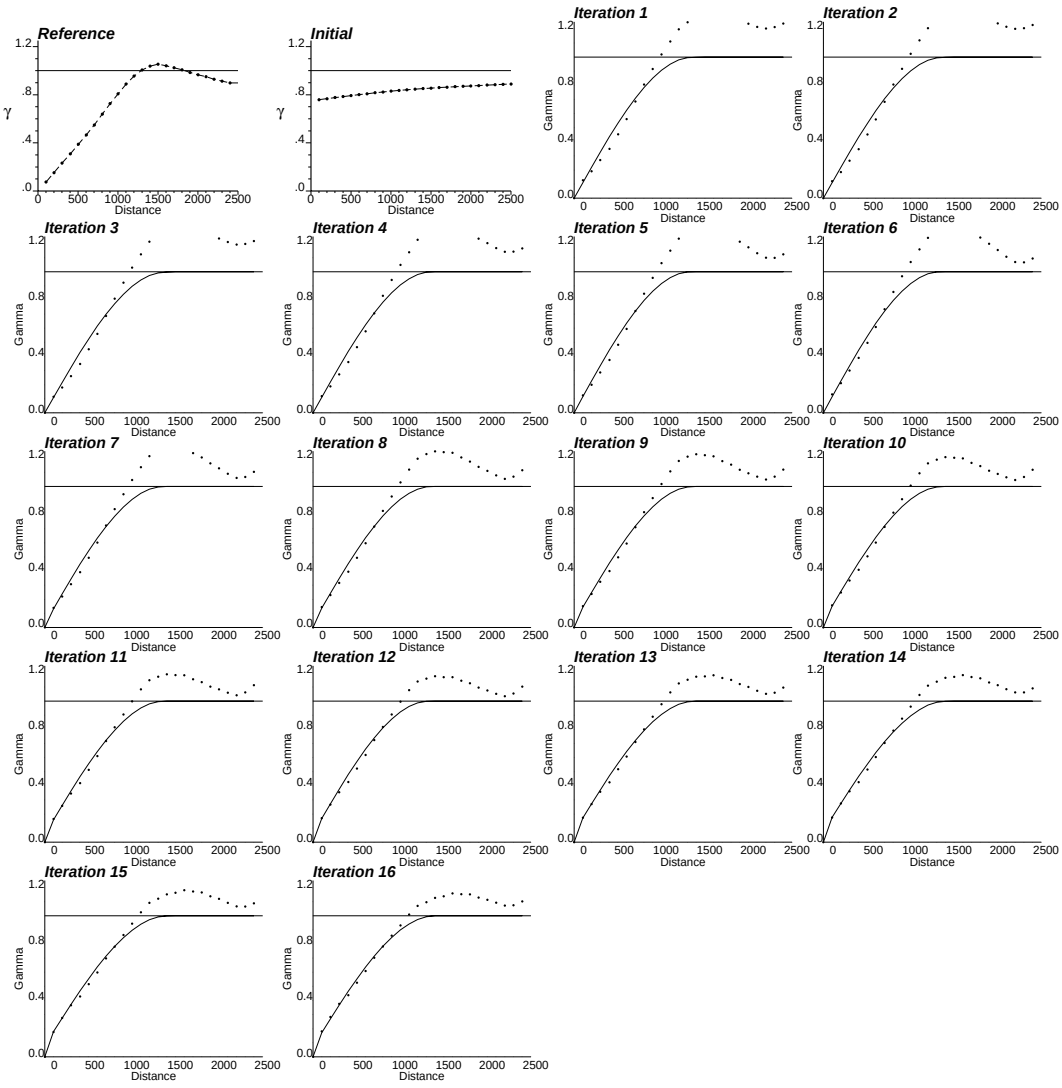


Figure 20: Reference, prior and updated variograms (experimental - dotted line, model - solid line) for $\ln(k)$ at each outer iteration: Example 1 Run 3. (Direction with azimuth 0)

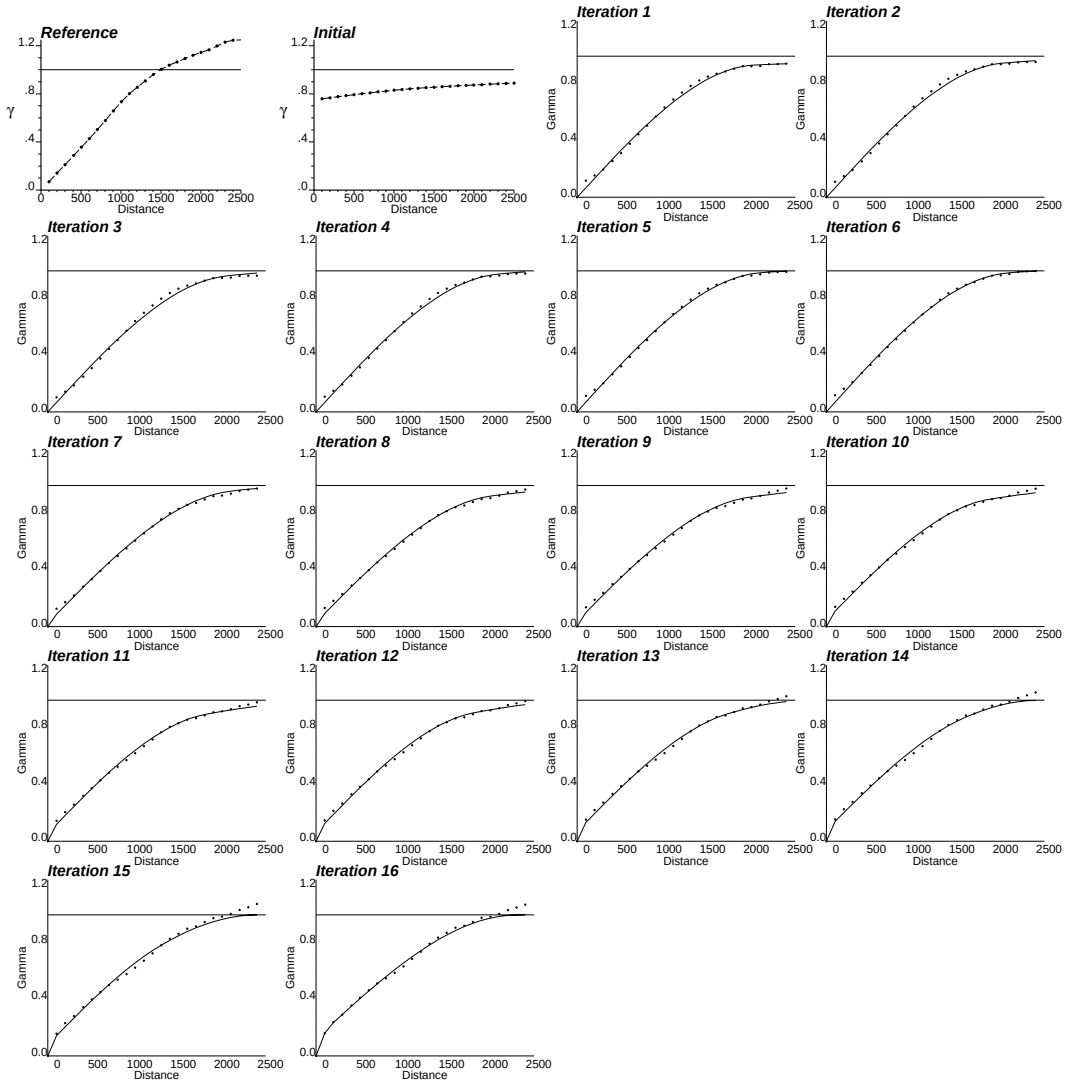


Figure 21: Reference, prior and updated variograms (experimental - dotted line, model - solid line) for $\ln(k)$ at each outer iteration: Example 1 Run 3. (Direction with azimuth 90)

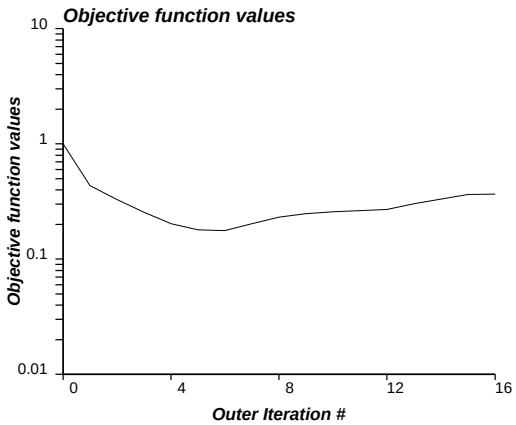


Figure 22: Mismatch norm of data integration at each outer iteration: Example 1 Run 3.

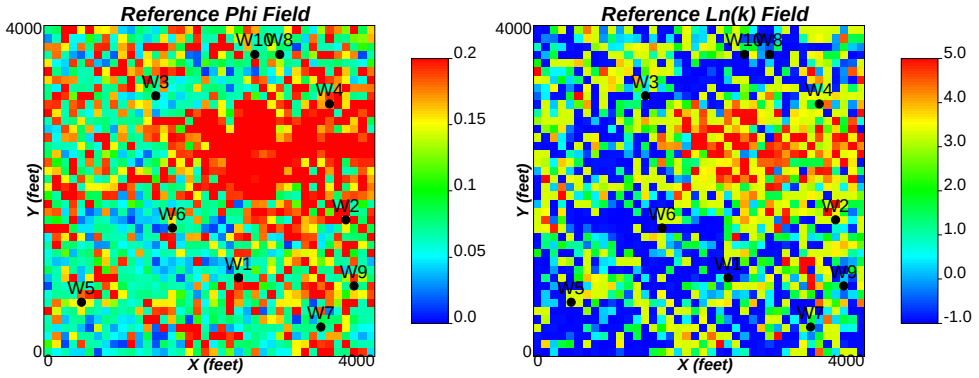


Figure 23: Reference $\phi$ and $\ln(k)$ fields: High Nugget Effect Example.

- Anisotropy convergence is also captured reasonably well in the final updated variogram models.

In the subsequent section, we will investigate the response of the developed code in the event of high nugget effect in the reference distribution. Given the diffusive nature of flow data, it would be interesting to see if the inversion algorithm can retrieve high spatial randomness in the reference distribution.

## High Nugget Effect Inversion Using Production Data

It is expected that inverted variogram models using production data will have very low nugget effect. The reason for such a hypothesis is the fact that subsurface reservoir fluid flow is diffusive in nature. Nevertheless, it would be interesting to perform some study of nugget effect inversion.

As in the earlier example, reference porosity and permeability models are constructed first. Pressure responses at a number of wells are obtained through flow simulation.

This 2D example of 4,000-ft square domain is discretized into 40 $\times$ 40 grid cells of 100 $\times$ 100 ft. Porosity and permeability fields are shown in Figure 23. There are 10 wells: Well W1 at the center of the cell (24,10), Wells W2, W3, W4, W5, W6, W7, W8, W9 and W10 at cells (37,17), (14,32), (35,31), (34,23), (28,13), (13,33), (16,29), (19,10), and (9,17), respectively. Wells are shown in Figure 23. Other reservoir properties are similar to the previous example. Figure 24 shows the imposed production rates and the corresponding numerically simulated pressure responses at the different wells. The histograms and the scatter-plot between $\phi$ and $\ln(k)$ are shown in Figures 25 and 26. Mean and standard deviation of reference distributions are 0.13 and 0.08 for $\phi$, and 1.38 and 2.06 for $\ln(k)$. Correlation coefficient of the two distributions is 0.658. Variogram for both $\phi$ and $\ln(k)$ of the reference fields are shown in Figure 27.

For the inversion, we employ the reference distributions as the global distribution information. Static well data used in the example are shown in Figure 28. Realistic experimental variograms could not be obtained using these static data.

The inversion was tried with a number of prior variogram models. It is not possible to capture high spatial randomness in the inverted distributions. We have employed prior variogram models with nugget effect from 0.05 to 0.75. In fact in the case of prior variogram models with low nugget effect, the mismatch function in the inversion increases instead of decreases. With a nugget effect of 0.75, inversion was possible however with a very poor mismatch of 47.3.

The prior variogram model used for the run with an initial nugget of 75% is shown in Tables 7 and 8 for $\phi$ and $\ln(k)$. The data integration code was run for 7 outer iterations using 6 $\times$ 6 (=36) master points in each iteration. CPU time for the run was only 157 seconds in a 1.8 GHz Pentium 4 personal computer. The updated variograms for $\phi$ and $\ln(k)$ are shown in Figures 29, 30, 31, and 32, for directions with azimuth 0 and 90. The mismatch in $L^2$ norms for each iteration is shown in Figure 33. The final $L^2$ norm of the pressure march was 47.3, an extremely high mismatch value. After 7 iterations, the final updated variogram models are given in Tables 9 and 10 for $\phi$ and $\ln(k)$.

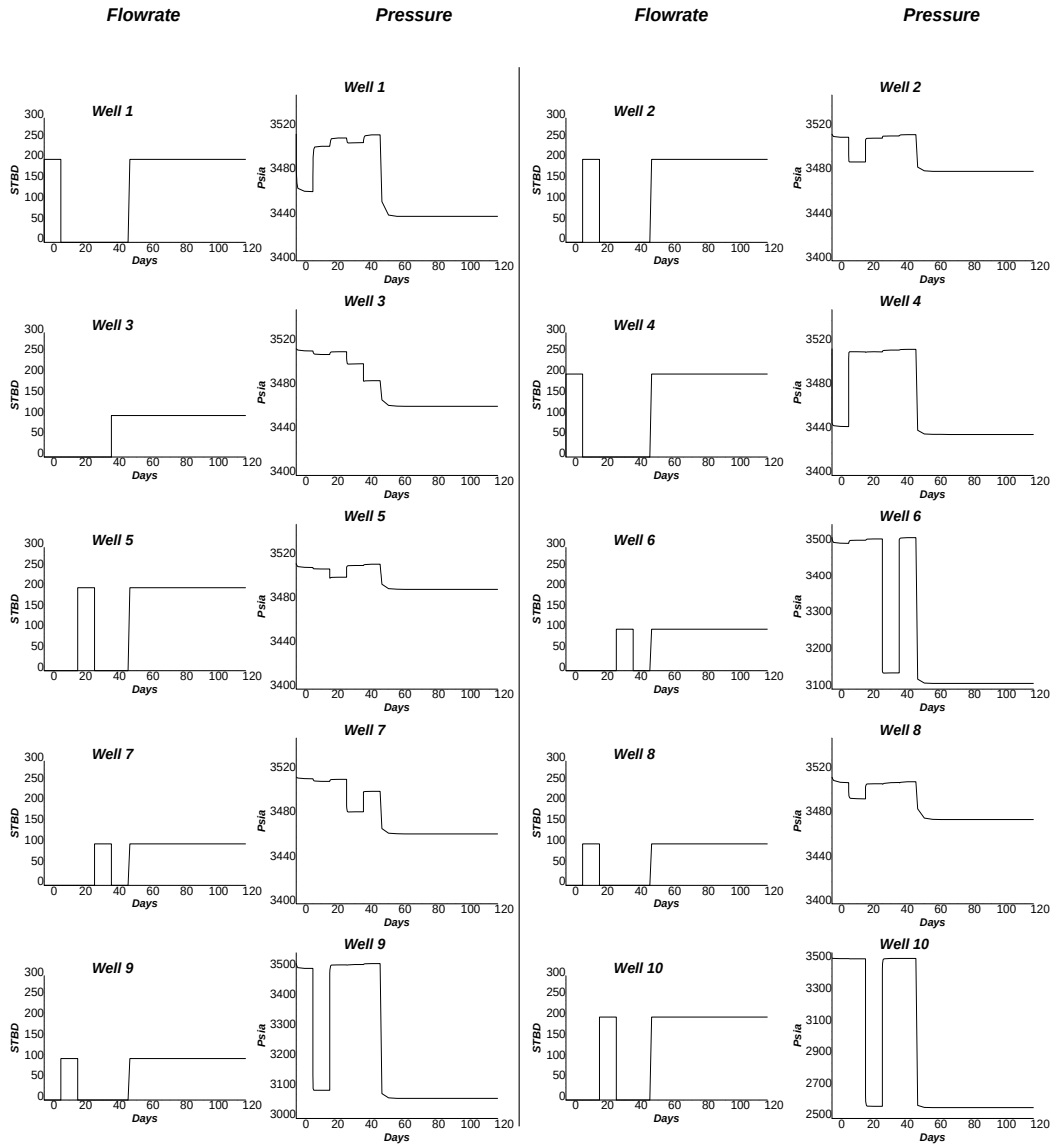


Figure 24: Production data (pressure and flow rates) obtained from the reference field: High Nugget Effect Example.

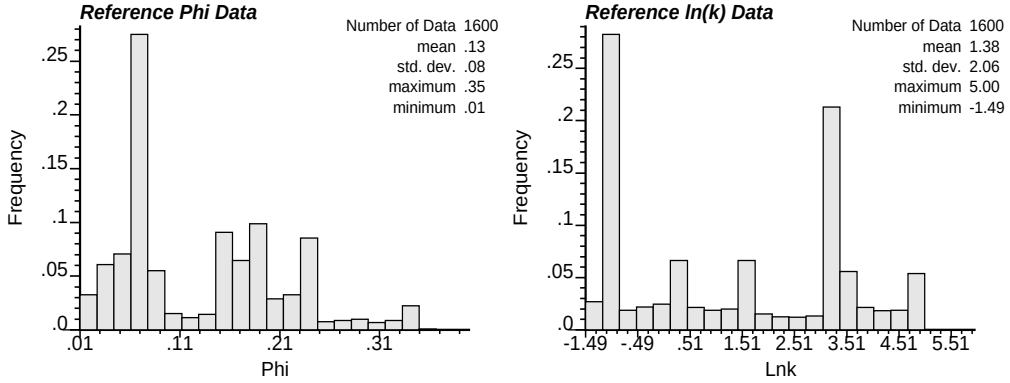


Figure 25: Histograms of reference $\phi$ and $\ln(k)$ fields: High Nugget Effect Example.

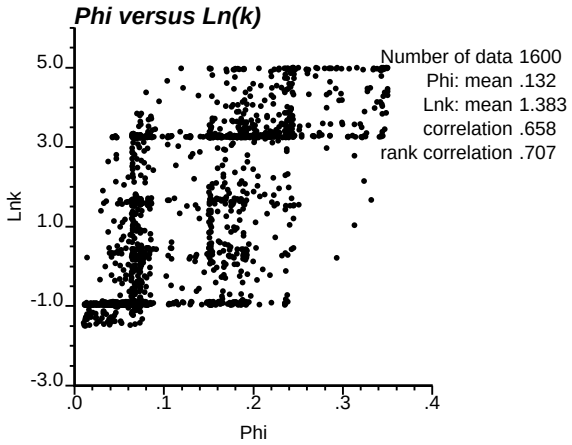


Figure 26: Scatterplot between reference $\phi$ and $\ln(k)$ values: High Nugget Effect Example.

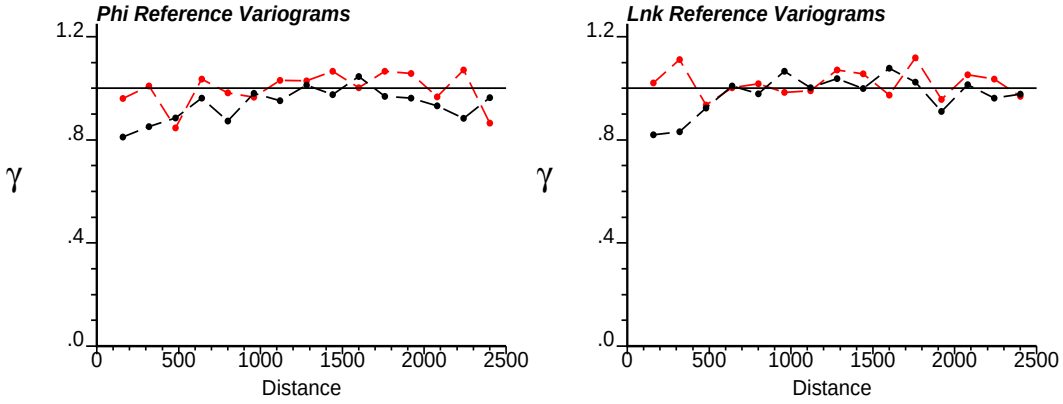


Figure 27: Variograms of reference $\phi$ and $\ln(k)$ distributions: High Nugget Effect Example. (X direction - dark, Y direction - light)

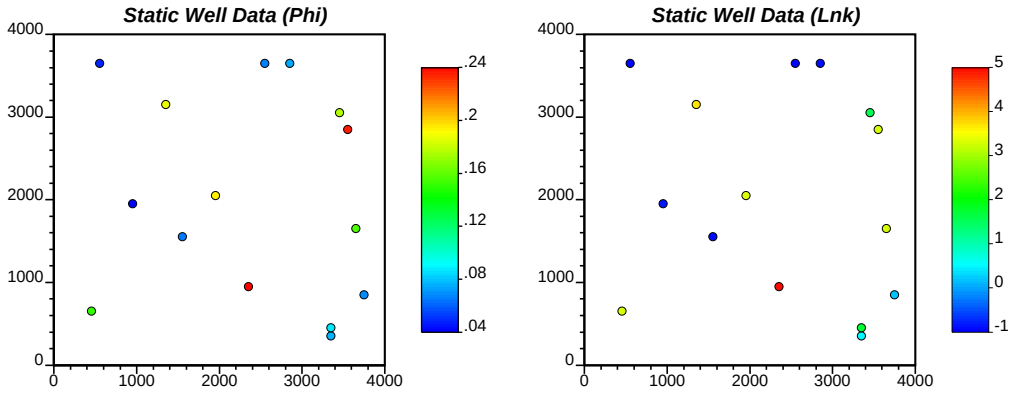


Figure 28: Static well data for $\phi$ and $\ln(k)$: High Nugget Effect Example.

| V. No. | Type | Sill | Range X - Y (ft) | Angle ($^o$) |
|---|---|---|---|---|
| 0 | Nugget | 0.05 | | |
| 1 | Sph | 0.5 | 7000 - 7000 | 0 |
| 2 | Sph | 0.45 | 4000 - 4000 | 0 |

Table 7: Prior variogram information used for $\phi$: High Nugget Effect Example.

| V. No. | Type | Sill | Range X - Y (ft) | Angle ($^o$) |
|---|---|---|---|---|
| 0 | Nugget | 0.05 | | |
| 1 | Sph | 0.55 | 3500 - 3500 | 0 |
| 2 | Sph | 0.4 | 6000 - 6000 | 0 |

Table 8: Prior variogram information used for $\ln(k)$: High Nugget Effect Example.

From the perspective of the geostatistical scaling laws in the context of small scale core data (perhaps with a nugget effect) and with block data (that is $10^4$ times larger), one would expect the nugget effect to smeared at the coarser scale. The heterogeneities one expects from production data integration are large scale caused by facies/stratigraphic boundaries or from faults. There really will be no nugget effect between "continuous" blocks. Moreover, even if we believed there was a nugget effect at the block scale, it would almost certainly be informed from densely spaced well log or core data. Our main task is to determine horizontal ranges and anisotropy (including perhaps, zonal anisotropy).

## Effect of Production Data

Variogram inversion requires production data having information about the reservoir heterogeneity. The amount of information captured in the inverted models depends on the quality and amount of production data. Here we investigate the effect of the quantity of dynamic data on updated variogram models.

We perform the inversion on a synthetic reservoir model with varying number of wells with production data. The updated variograms models are compared and analyzed to determine the effect of the amount of production data on the resulting variogram.

Consider our familiar 2D 4,000-ft square domain discretized into $40 \times 40$ grid cells of $100 \times 100$ ft. Porosity and permeability fields are shown in Figure 34. The boundaries on all four sides are no-flow boundaries. Reservoir properties are the same as those discussed in the previous sections unless stated otherwise. There is a high porosity-permeability band connecting the lower-left corner and upper-right corner. The histograms and the scatter-plot between $\phi$ and $\ln(k)$ are shown in Figures 35 and 36. The distribution is bimodal. The correlation coefficient of the two distributions is 1.0. Mean and standard deviation of reference distributions are 0.13 and 0.046 for $\phi$, and 0.683 and 2.108 for $\ln(k)$. Variogram for both $\phi$ and $\ln(k)$ of the reference fields are shown in Figure 37. We employ the reference distributions as the global distribution information. The prior variogram model used in this exercise is shown in Tables 11 and 12 for $\phi$ and $\ln(k)$.

We perform the inversion 3 times with production data from 4, 6 and 8 wells. The well locations for each case are shown in Figure 38. Figures 39, 40, and 41 show the imposed production rates and

| V. No. | Type | Sill | Range X - Y (ft) | Angle ($^o$) |
|---|---|---|---|---|
| 0 | Nugget | 0.0 | | |
| 1 | Sph | 0.95 | 1825 - 2049 | 0 |
| 2 | Sph | 0.05 | 1800 - 2016 | 0 |

Table 9: Final variogram model obtained for $\phi$ after 7 iterations: High Nugget Effect Example.

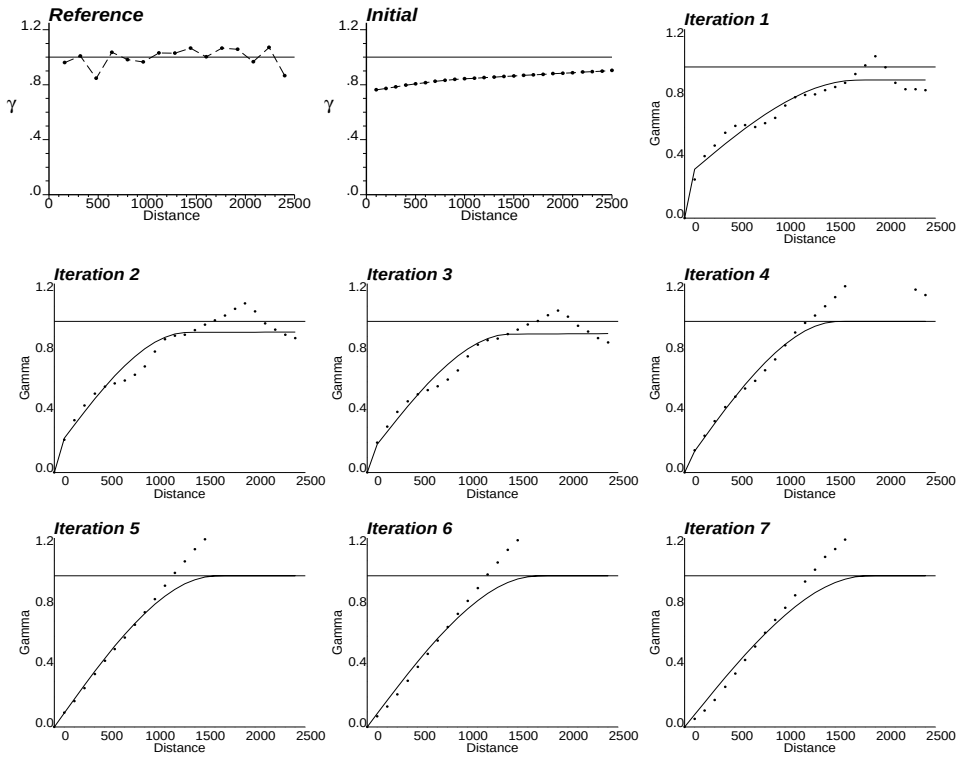


Figure 29: Reference, prior and updated variograms (experimental - dotted line, model - solid line) for $\phi$ at each outer iteration: High Nugget Effect Example. (Direction with azimuth 0)

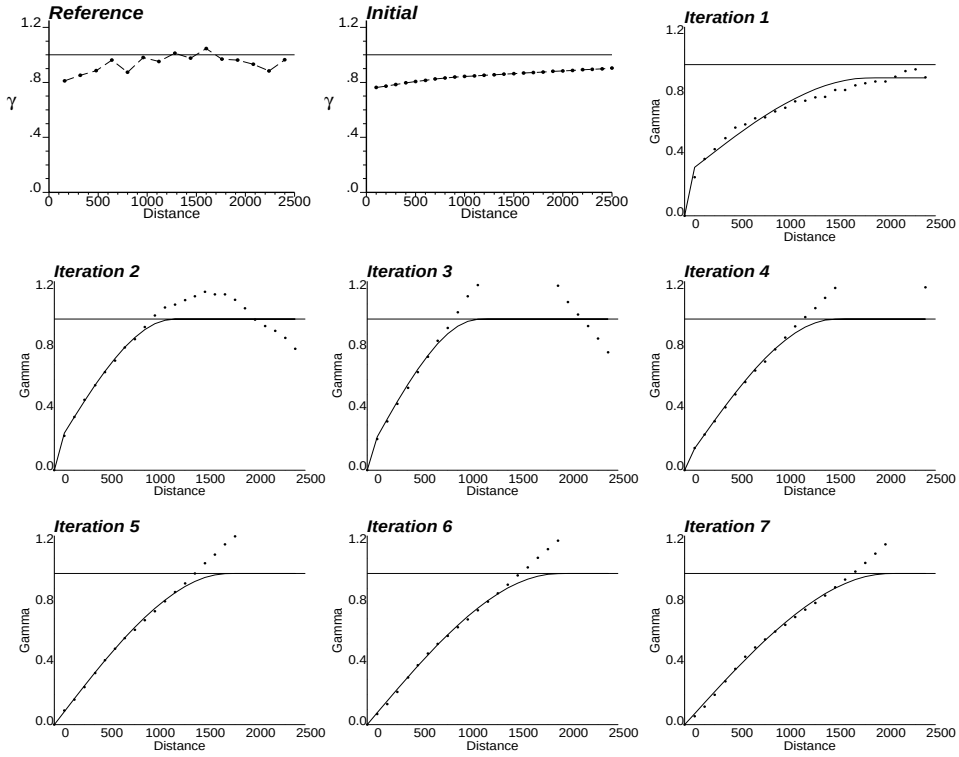


Figure 30: Reference, prior and updated variograms (experimental - dotted line, model - solid line) for $\phi$ at each outer iteration: High Nugget Effect Example. (Direction with azimuth 90)

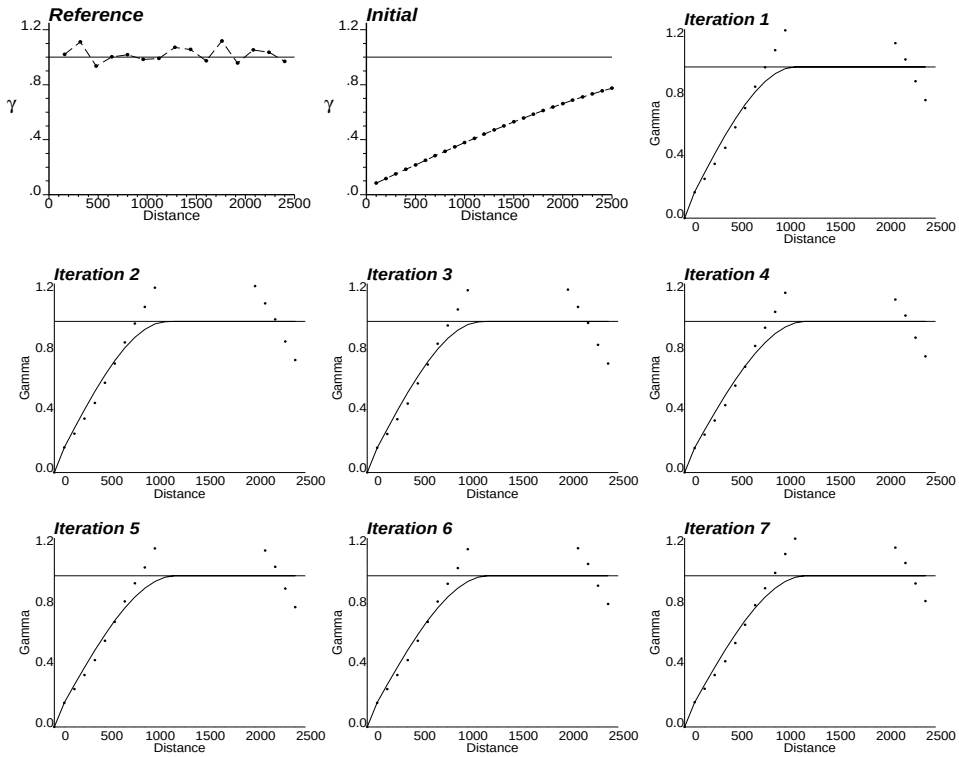


Figure 31: Reference, prior and updated variograms (experimental - dotted line, model - solid line) for $\ln(k)$ at each outer iteration: High Nugget Effect Example. (Direction with azimuth 0)

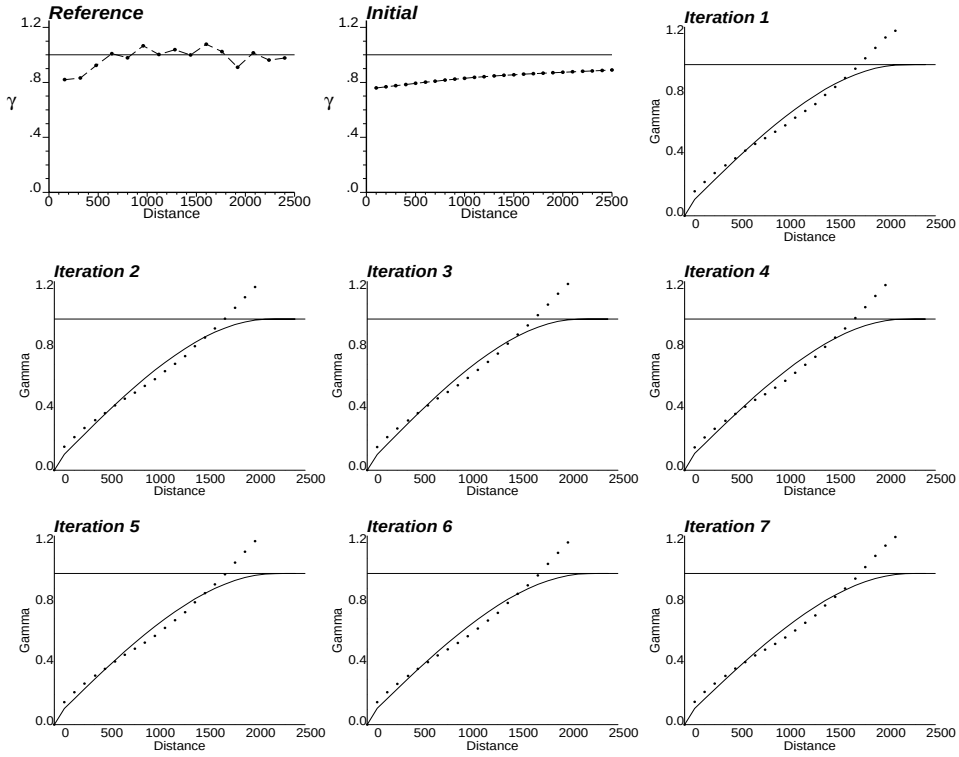


Figure 32: Reference, prior and updated variograms (experimental - dotted line, model - solid line) for $\ln(k)$ at each outer iteration: High Nugget Effect Example. (Direction with azimuth 90)

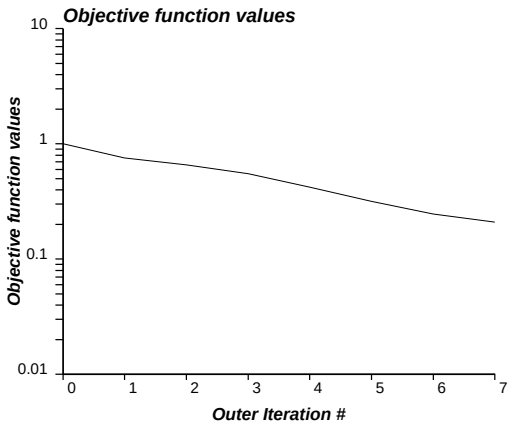


Figure 33: Mismatch norm of data integration at each outer iteration: High Nugget Effect Example.

| V. No. | Type | Sill | Range X - Y (ft) | Angle ($^o$) |
|---|---|---|---|---|
| 0 | Nugget | 0.044 | | |
| 1 | Sph | 0.593 | 1200 - 2268 | 0 |
| 2 | Sph | 0.363 | 1200 - 2232 | 0 |

Table 10: Final variogram model obtained for $\ln(k)$ after 7 iterations: High Nugget Effect Example.

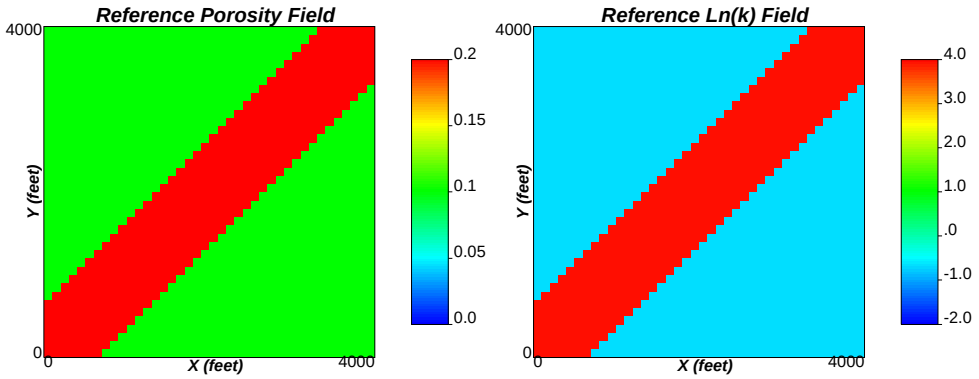


Figure 34: Reference $\phi$ and $\ln(k)$ fields: Production Data Sensitivity Example.

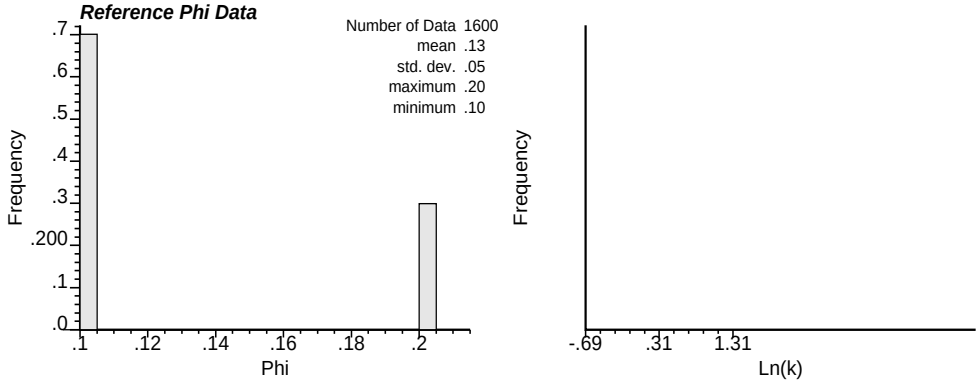


Figure 35: Histograms of reference $\phi$ and $\ln(k)$ fields: Production Data Sensitivity Example.

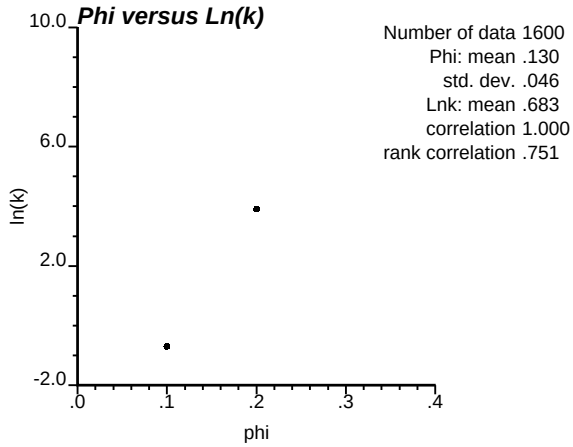


Figure 36: Scatterplot between reference $\phi$ and $\ln(k)$ values: Production Data Sensitivity Example.

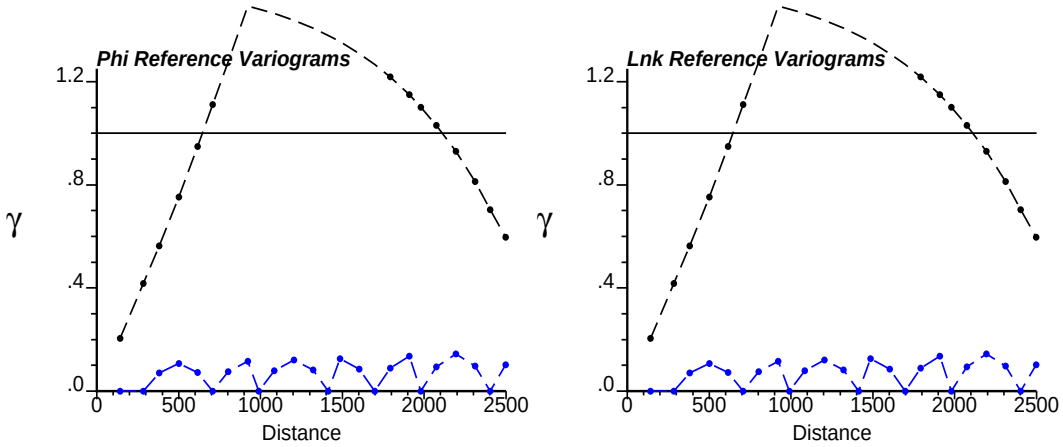


Figure 37: Variograms of reference $\phi$ and $\ln(k)$ distributions: Production Data Sensitivity Example. (X direction - dark, Y direction - light)

| **V. No.** | **Type** | **Sill** | **Range** X - Y (ft) | **Angle** ($^o$) |
|---|---|---|---|---|
| 0 | Nugget | 0.05 | | |
| 1 | Sph | 0.55 | 14000 - 2000 | 45.0 |
| 2 | Sph | 0.4 | 13000 - 10000 | 45.0 |

Table 11: Prior variogram information used for $\phi$: Production Data Sensitivity Example.

| **V. No.** | **Type** | **Sill** | **Range** X - Y (ft) | **Angle** ($^o$) |
|---|---|---|---|---|
| 0 | Nugget | 0.05 | | |
| 1 | Sph | 0.5 | 14000 - 2000 | 45.0 |
| 2 | Sph | 0.45 | 13000 - 10000 | 45.0 |

Table 12: Prior variogram information used for $\ln(k)$: Production Data Sensitivity Example.

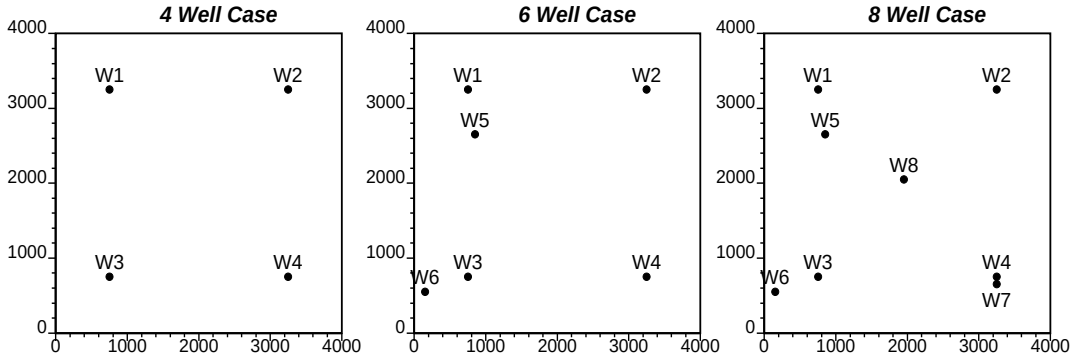


Figure 38: Well locations for the 3 cases: 4, 6 and 8 well case.

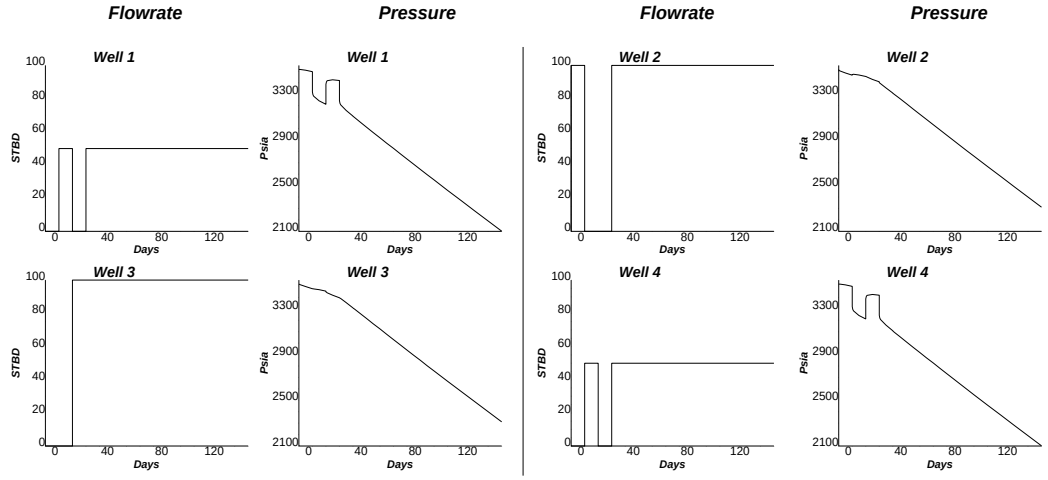


Figure 39: Production data (pressure and flow rates) obtained from the reference field: 4 well case.

the corresponding numerically simulated pressure responses for the 3 cases. Only the well porosity and permeability values are used for the inversion.

## 4 Well Case

The inversion was performed for 11 outer iterations. CPU time for the run was only 213 seconds in a 1.8 GHz Pentium 4 personal computer. The updated variograms for $\phi$ and $\ln(k)$ are shown in Figures 42, 43, 44, and 45, for directions with azimuth 45 and 135. The mismatch in $L^2$ norms for each iteration is shown in Figure 46. The final $L^2$ norm of the pressure march was 10.91. After 11 iterations, the final updated variogram models are given in Tables 13 and 14 for $\phi$ and $\ln(k)$.

| **V. No.** | **Type** | **Sill** | **Range** X - Y (ft) | **Angle** ($^o$) |
|---|---|---|---|---|
| 0 | Nugget | 0.0 | | |
| 1 | Sph | 0.555 | 2787 - 983 | 45 |
| 2 | Sph | 0.445 | 925 - 194 | 45 |

Table 13: Final variogram model obtained for $\phi$ after 11 iterations: 4 Well case.

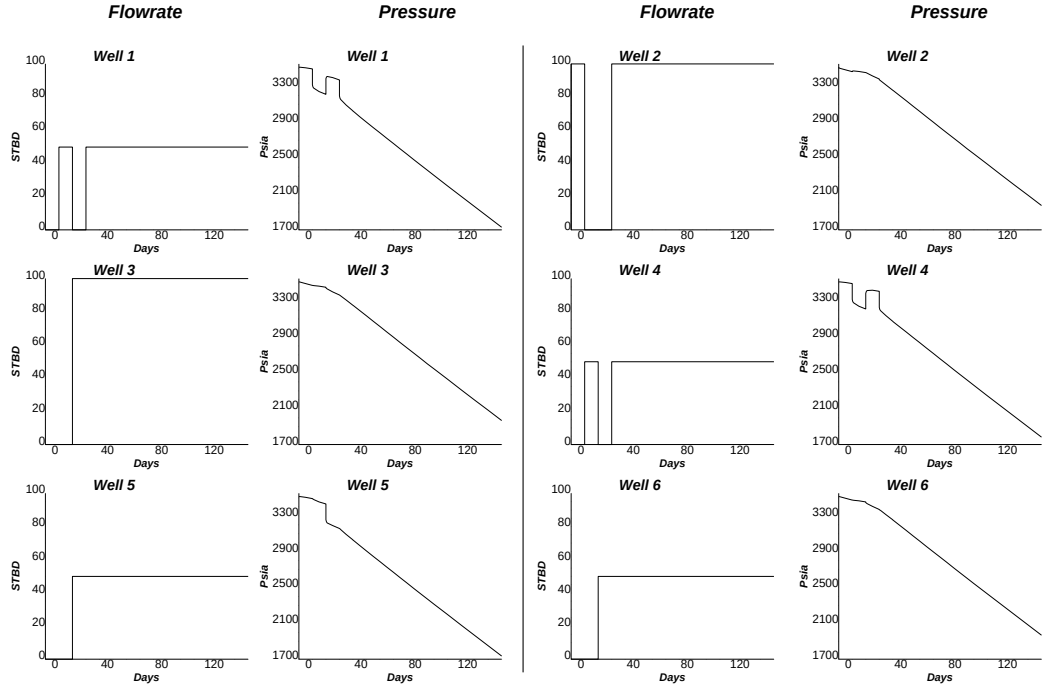


Figure 40: Production data (pressure and flow rates) obtained from the reference field: 6 well case.

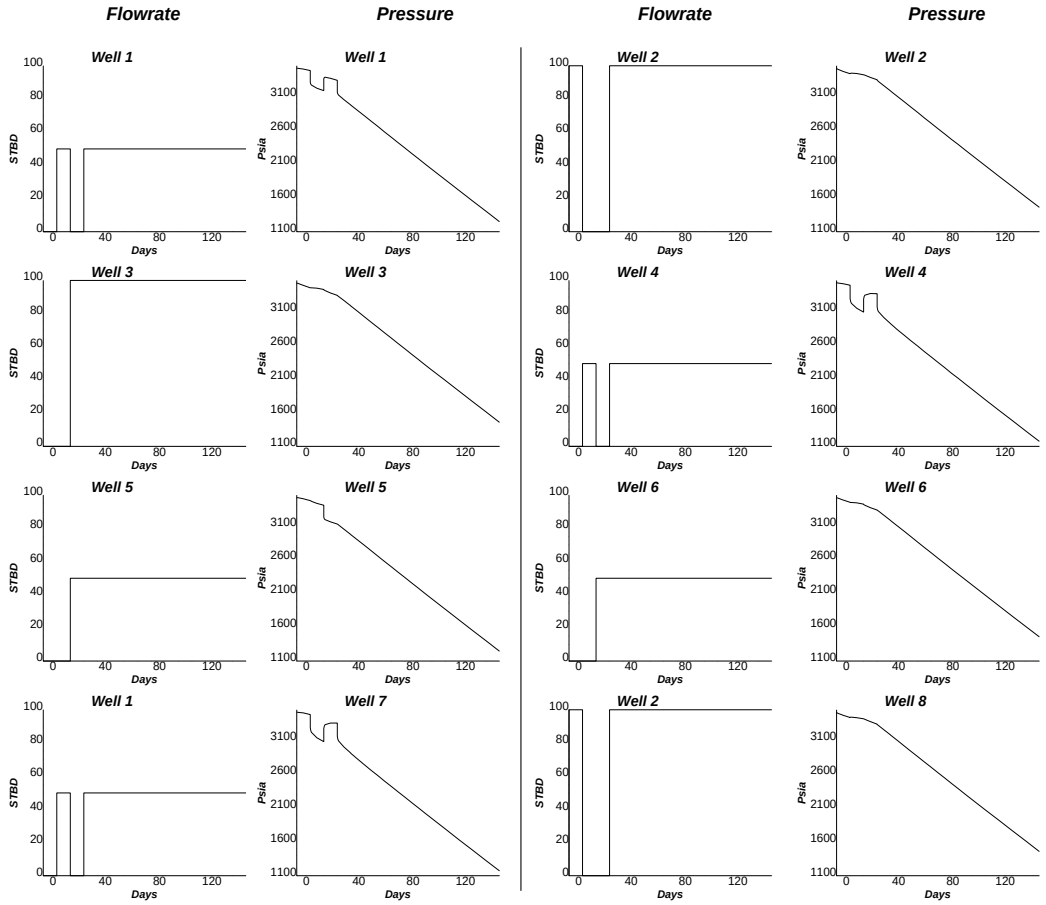


Figure 41: Production data (pressure and flow rates) obtained from the reference field: 8 well case.

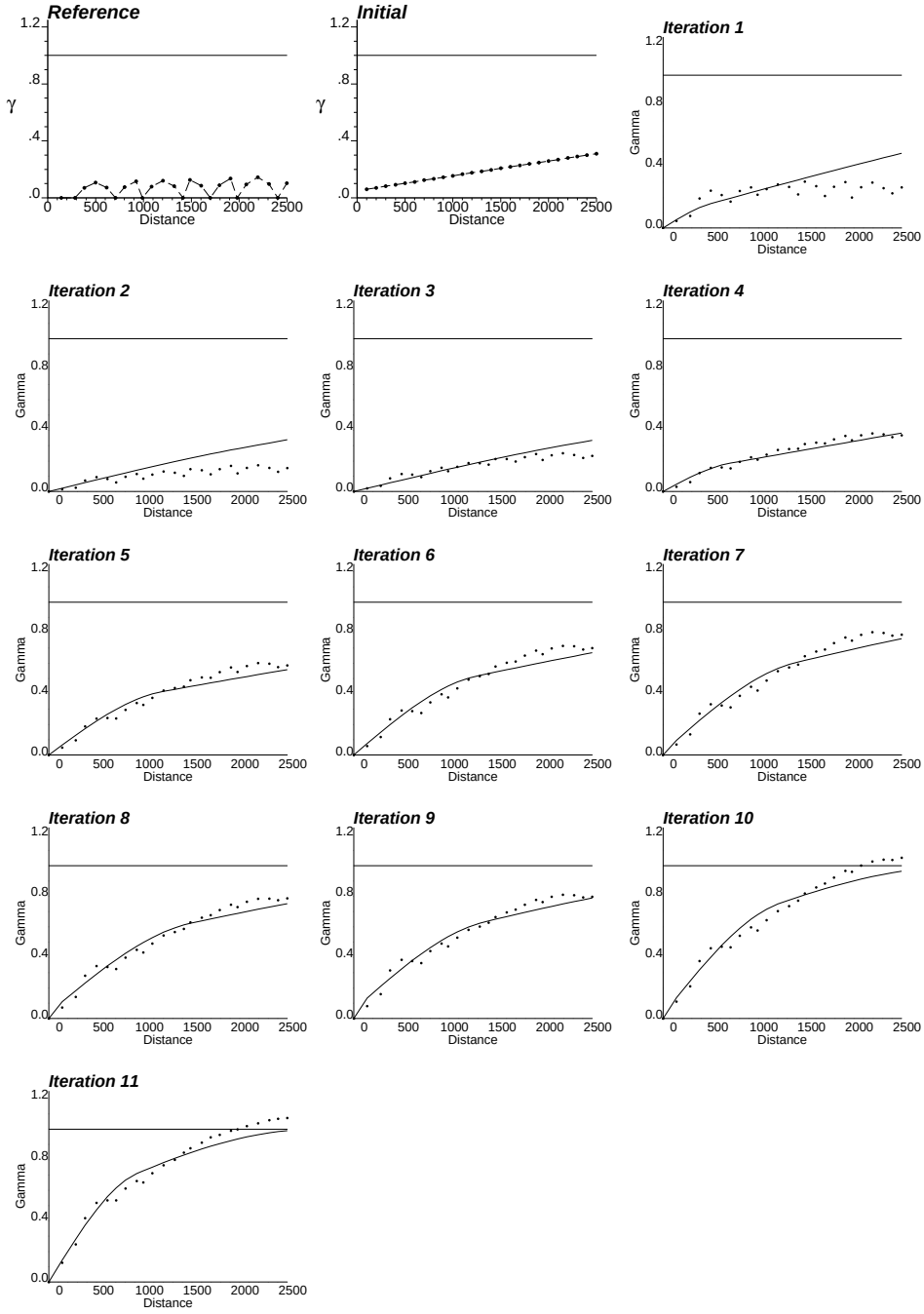


Figure 42: Reference, prior and updated variograms (experimental - dotted line, model - solid line) for $\phi$ at each outer iteration: 4 Well case. (Direction with azimuth 45)

| **V. No.** | **Type** | **Sill** | **Range** X - Y (ft) | **Angle** ($^o$) |
|---|---|---|---|---|
| 0 | Nugget | 0.003 | | |
| 1 | Sph | 0.86 | 10900 - 903 | 45 |
| 2 | Sph | 0.137 | 2600 - 895 | 45 |

Table 14: Final variogram model obtained for $\ln(k)$ after 11 iterations: 4 Well case.

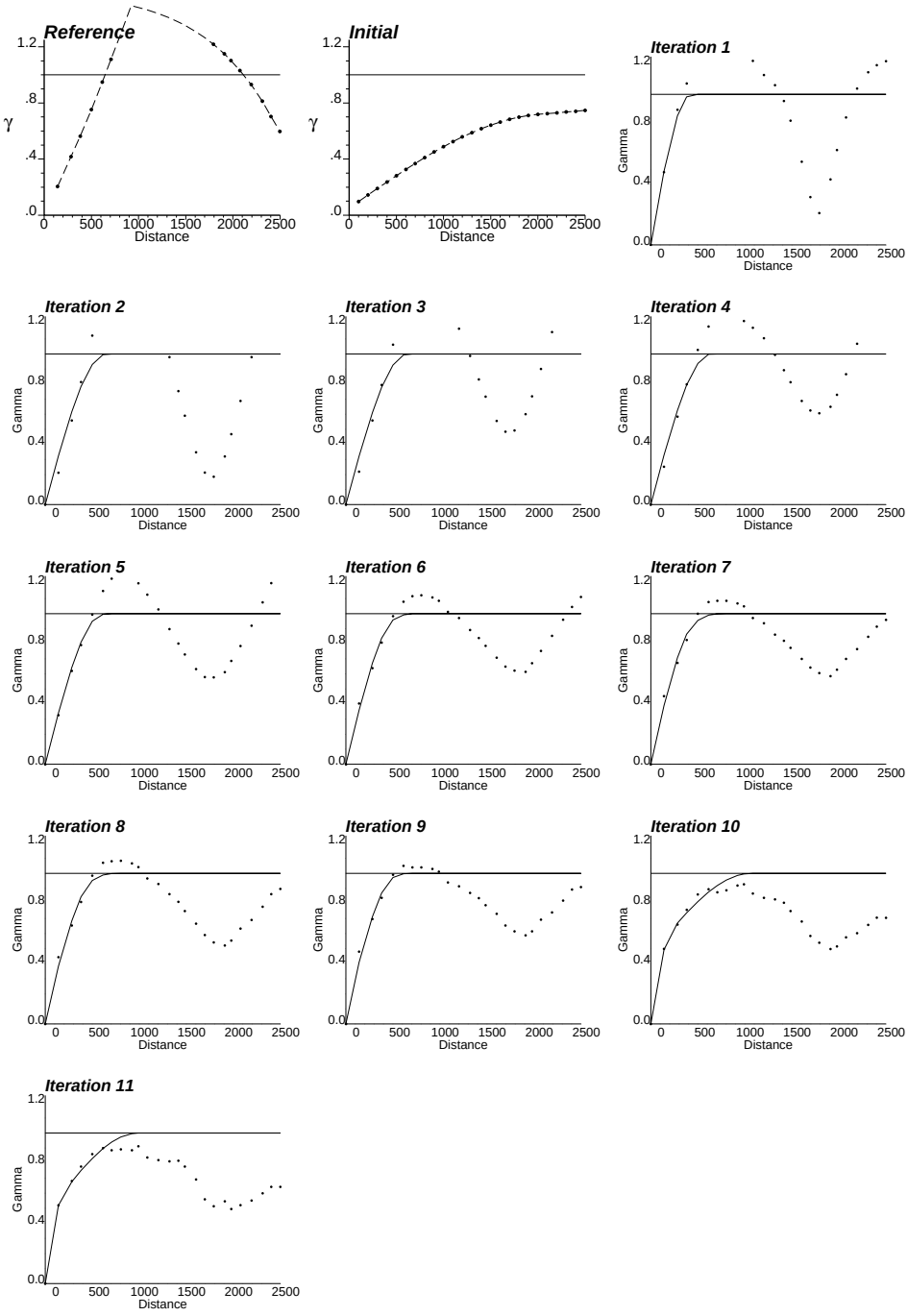


Figure 43: Reference, prior and updated variograms (experimental - dotted line, model - solid line) for $\phi$ at each outer iteration: 4 Well case. (Direction with azimuth 135)

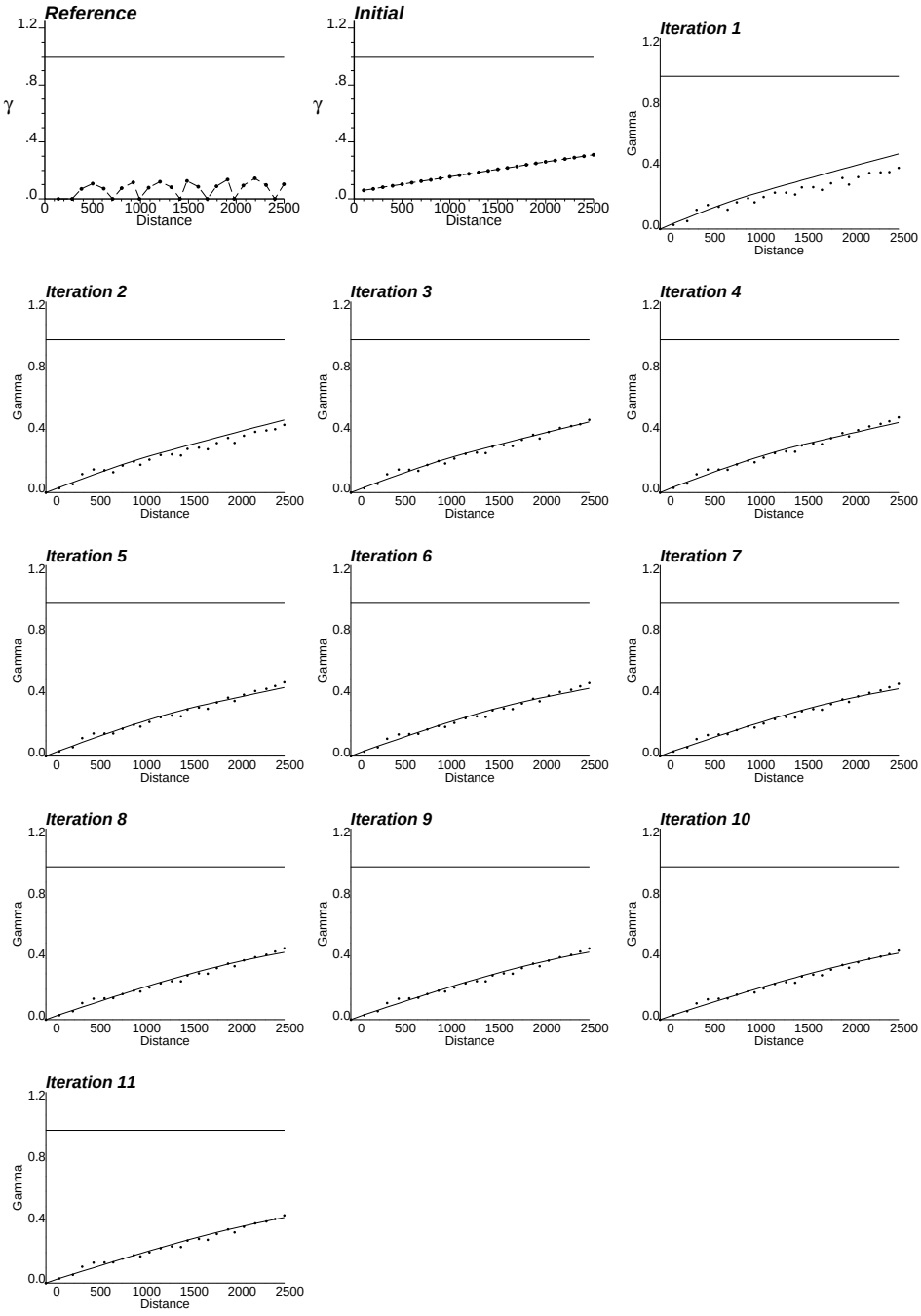


Figure 44: Reference, prior and updated variograms (experimental - dotted line, model - solid line) for $\ln(k)$ at each outer iteration: 4 Well case. (Direction with azimuth 45)

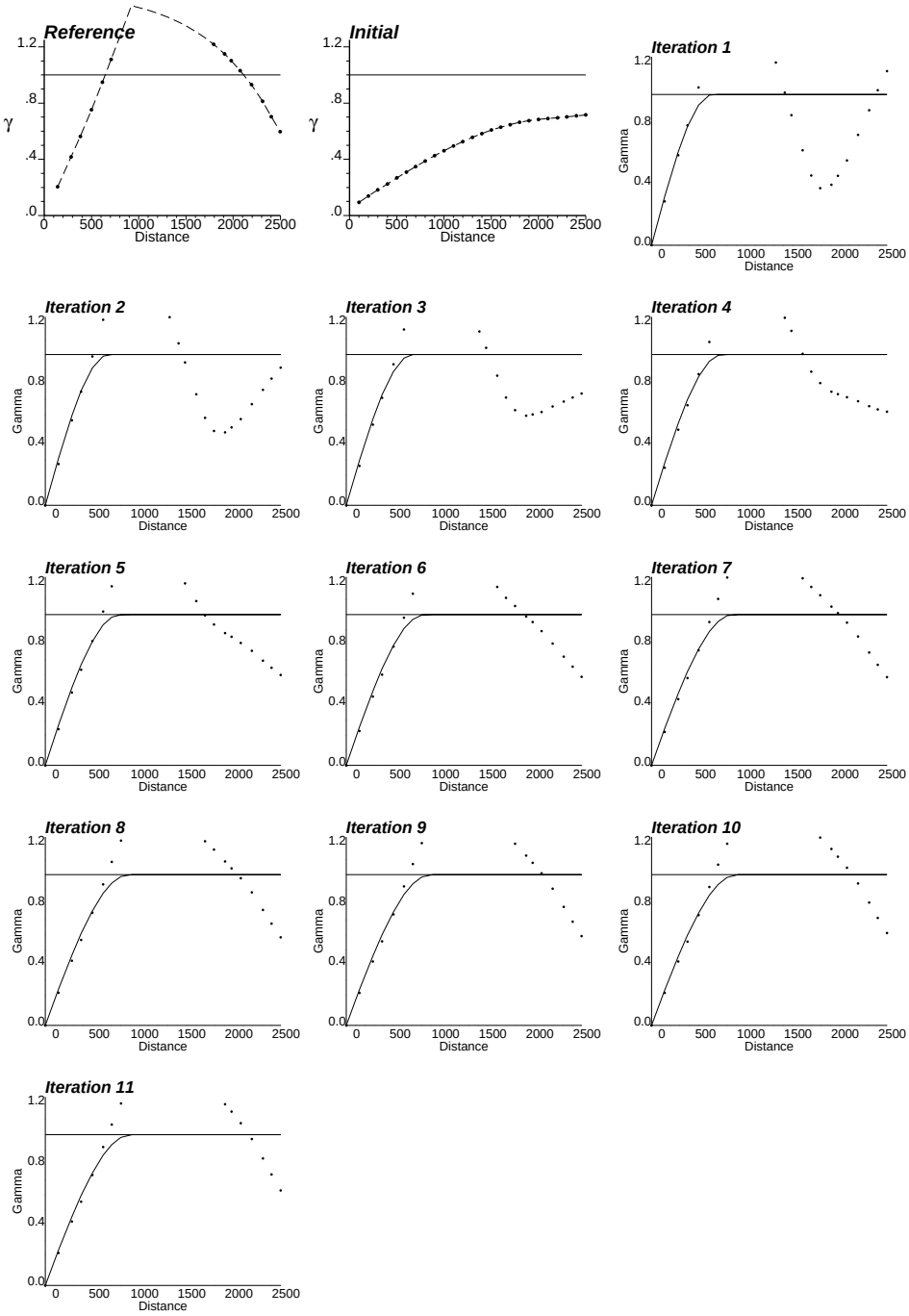


Figure 45: Reference, prior and updated variograms (experimental - dotted line, model - solid line) for $\ln(k)$ at each outer iteration: 4 Well case. (Direction with azimuth 135)

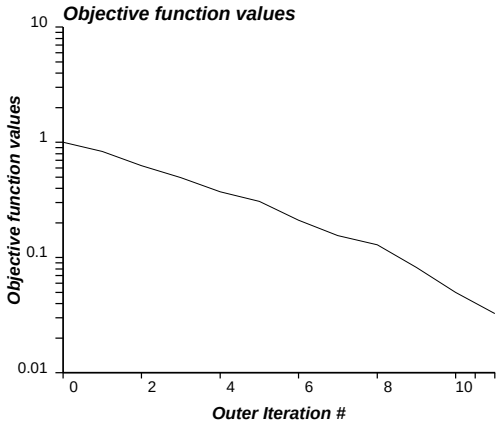


Figure 46: Mismatch norm of data integration at each outer iteration: 4 Well case.

| **V. No.** | **Type** | **Sill** | **Range** X - Y (ft) | **Angle** ($^o$) |
|---|---|---|---|---|
| 0 | Nugget | 0.001 | | |
| 1 | Sph | 0.575 | 10650 - 669 | 45 |
| 2 | Sph | 0.424 | 500 - 31 | 45 |

Table 15: Final variogram model obtained for $\phi$ after 13 iterations: 6 Well case.

## 6 Well Case

The inversion was performed for 13 outer iterations. CPU time for the run was only 252 seconds in a 1.8 GHz Pentium 4 personal computer. The updated variograms for $\phi$ and $\ln(k)$ are shown in Figures 47, 48, 49, and 50, for directions with azimuth 45 and 135. The mismatch in $L^2$ norms for each iteration is shown in Figure 51. The final $L^2$ norm of the pressure march was 11.39. After 13 iterations, the final updated variogram models are given in Tables 15 and 16 for $\phi$ and $\ln(k)$.

## 8 Well Case

The inversion was performed for 10 outer iterations. CPU time for the run was only 195 seconds in a 1.8 GHz Pentium 4 personal computer. The updated variograms for $\phi$ and $\ln(k)$ are shown in Figures 52, 53, 54, and 55, for directions with azimuth 45 and 135. The mismatch in $L^2$ norms for each iteration is shown in Figure 56. The final $L^2$ norm of the pressure march was 27.34. After 10 iterations, the final updated variogram models are given in Tables 17 and 18 for $\phi$ and $\ln(k)$.

## Some Conclusions on Effect of Production Data

Production data contains information about reservoir heterogeneity. The question is how much information we can retrieve with our developed algorithm. Having analyzed the responses, we can definitely improve the variogram parameters using production data. Some of the observations are the following.

- Variogram inversion for $\ln(k)$ is relatively better than that for $\phi$.

| **V. No.** | **Type** | **Sill** | **Range** X - Y (ft) | **Angle** ($^o$) |
|---|---|---|---|---|
| 0 | Nugget | 0.001 | | |
| 1 | Sph | 0.933 | 13100 - 922 | 45 |
| 2 | Sph | 0.066 | 450 - 72 | 45 |

Table 16: Final variogram model obtained for $\ln(k)$ after 13 iterations: 6 Well case.

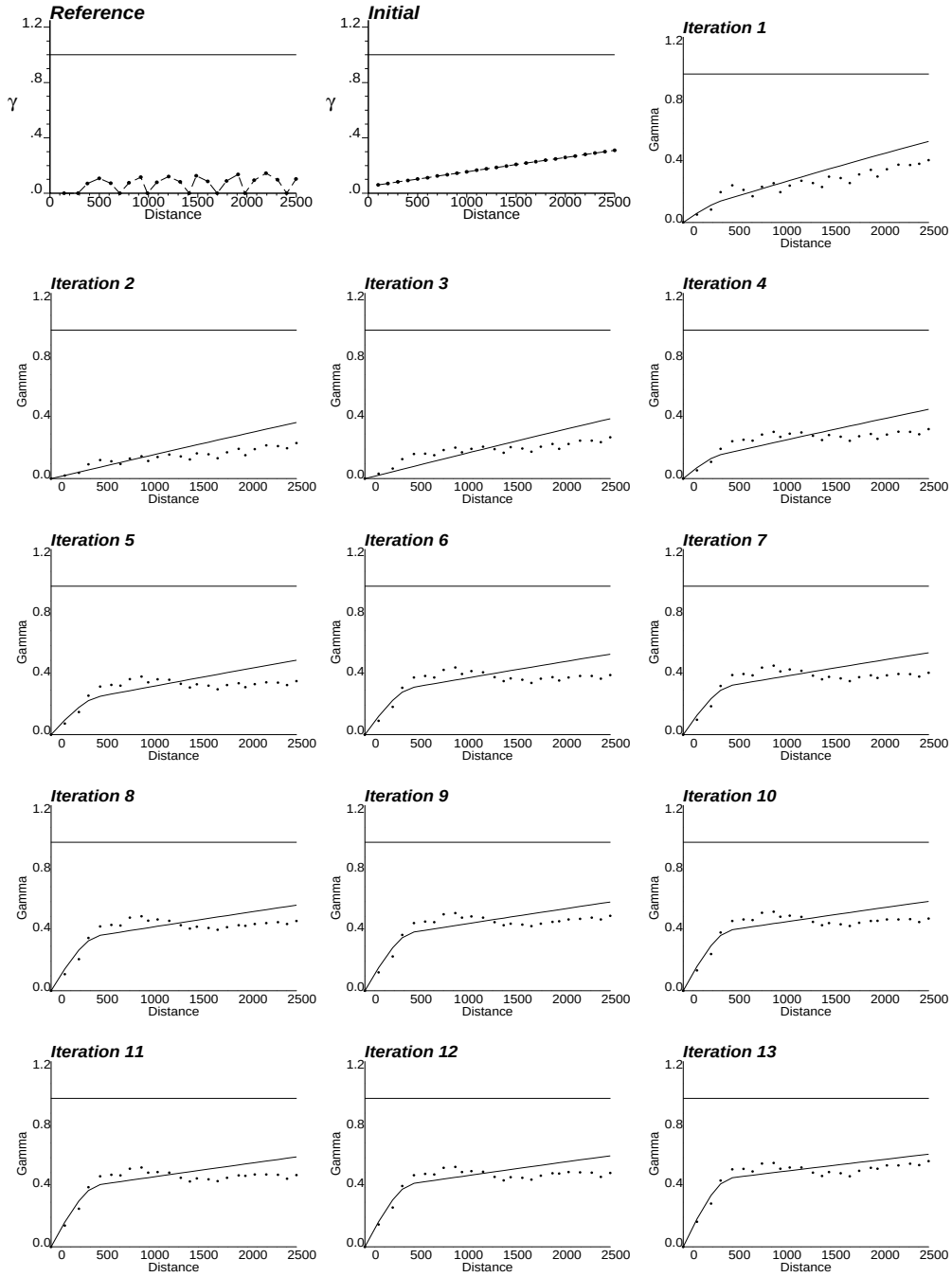


Figure 47: Reference, prior and updated variograms (experimental - dotted line, model - solid line) for $\phi$ at each outer iteration: 6 Well case. (Direction with azimuth 45)

| **V. No.** | **Type** | **Sill** | **Range** X - Y (ft) | **Angle** ($^o$) |
|---|---|---|---|---|
| 0 | Nugget | 0.0 | | |
| 1 | Sph | 0.339 | 575 - 220 | 45 |
| 2 | Sph | 0.661 | 10050 - 545 | 45 |

Table 17: Final variogram model obtained for $\phi$ after 10 iterations: 8 Well case.

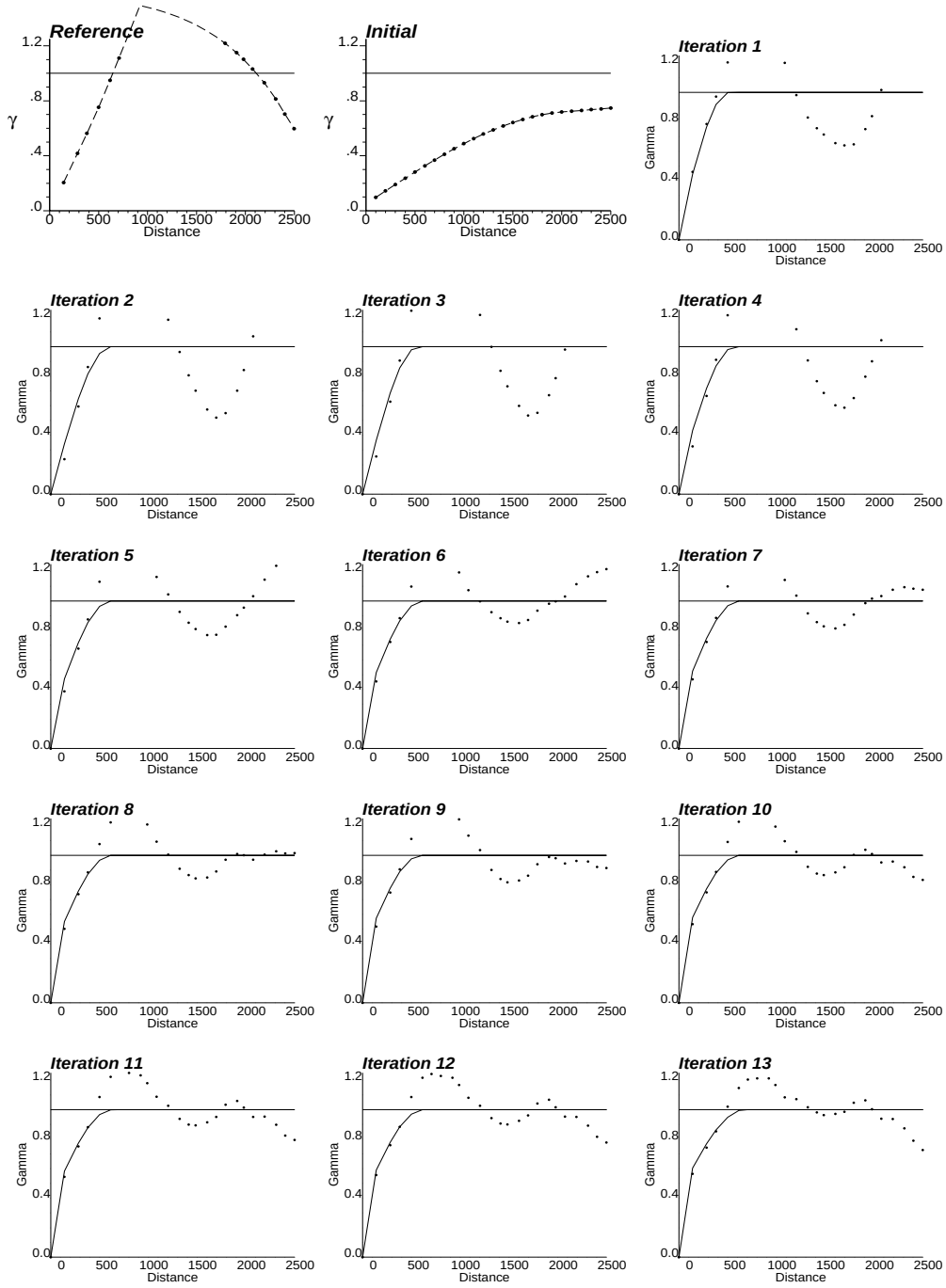


Figure 48: Reference, prior and updated variograms (experimental - dotted line, model - solid line) for $\phi$ at each outer iteration: 6 Well case. (Direction with azimuth 135)

| **V. No.** | **Type** | **Sill** | **Range** X - Y (ft) | **Angle** ($^o$) |
|---|---|---|---|---|
| 0 | Nugget | 0.003 | | |
| 1 | Sph | 0.903 | 12000 - 934 | 45 |
| 2 | Sph | 0.094 | 600 - 96 | 45 |

Table 18: Final variogram model obtained for $\ln(k)$ after 10 iterations: 8 Well case.

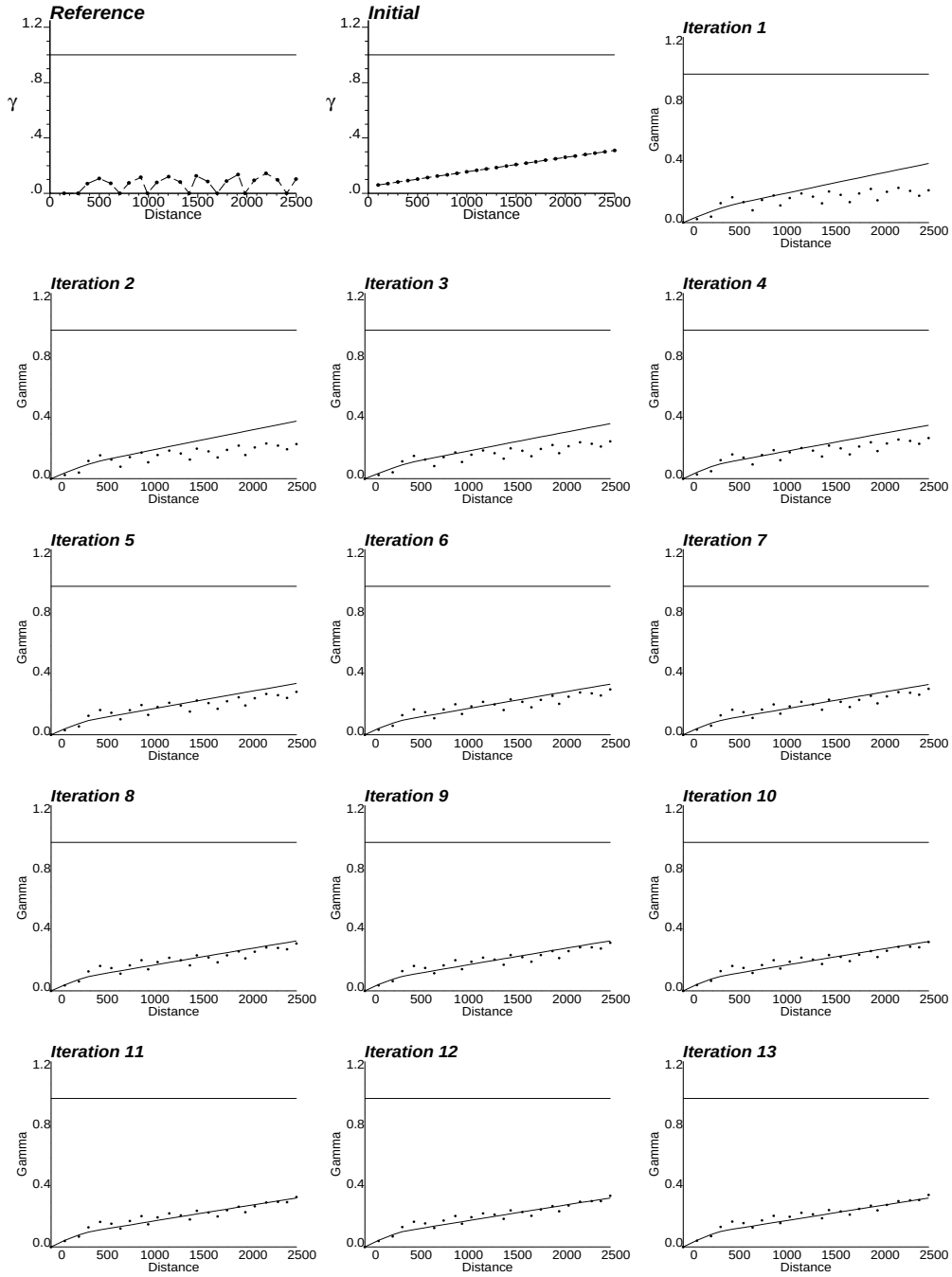


Figure 49: Reference, prior and updated variograms (experimental - dotted line, model - solid line) for $\ln(k)$ at each outer iteration: 6 Well case. (Direction with azimuth 45)

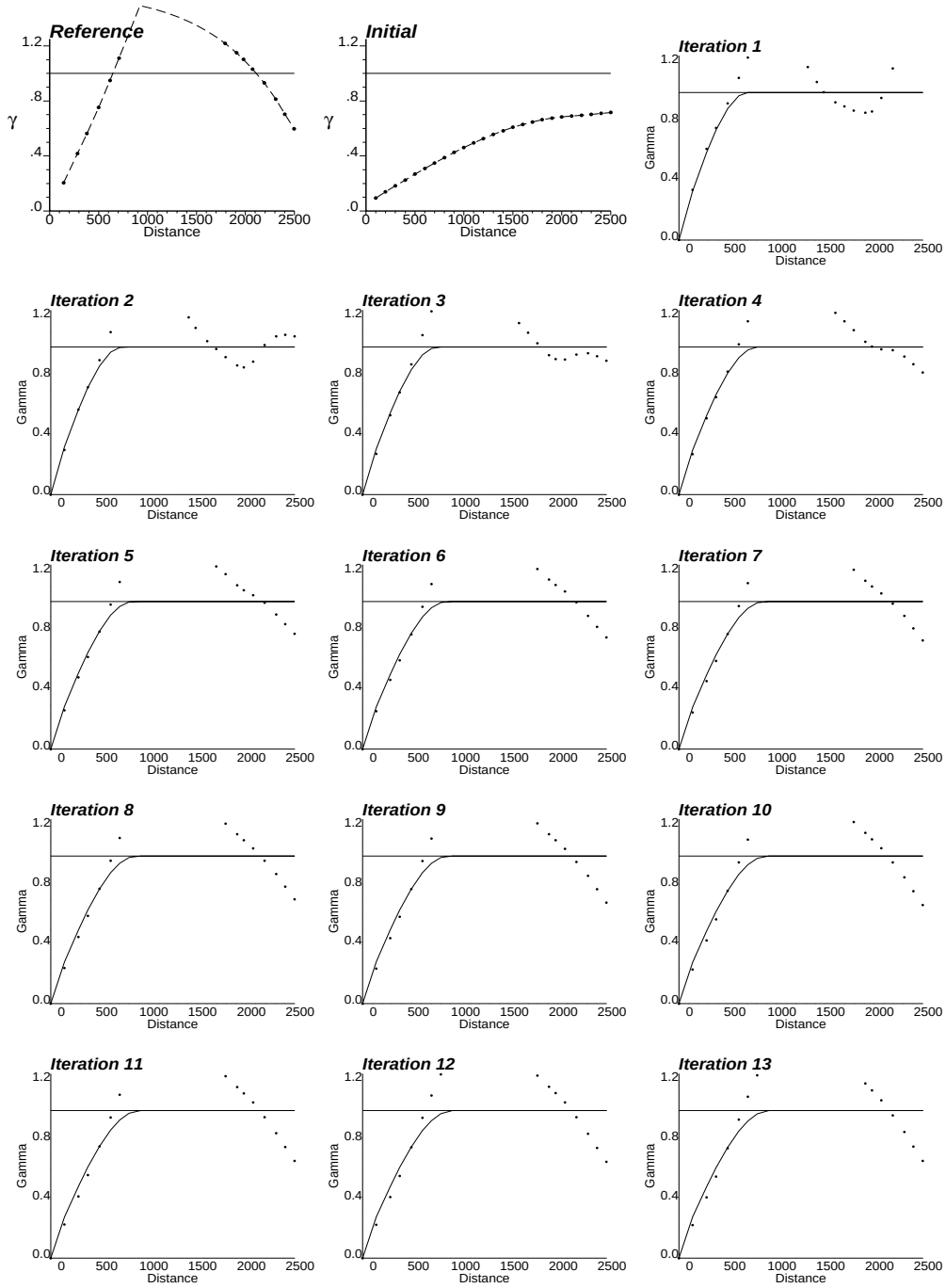


Figure 50: Reference, prior and updated variograms (experimental - dotted line, model - solid line) for $\ln(k)$ at each outer iteration: 6 Well case. (Direction with azimuth 135)

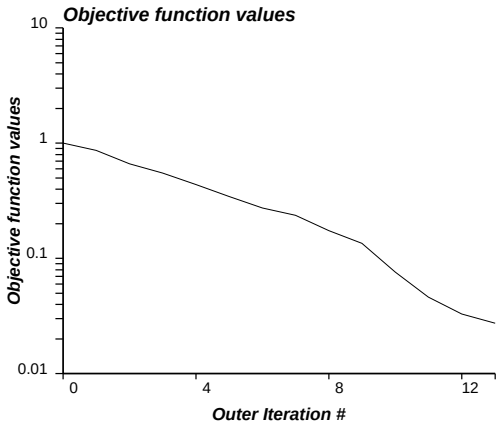


Figure 51: Mismatch norm of data integration at each outer iteration: 6 Well case.

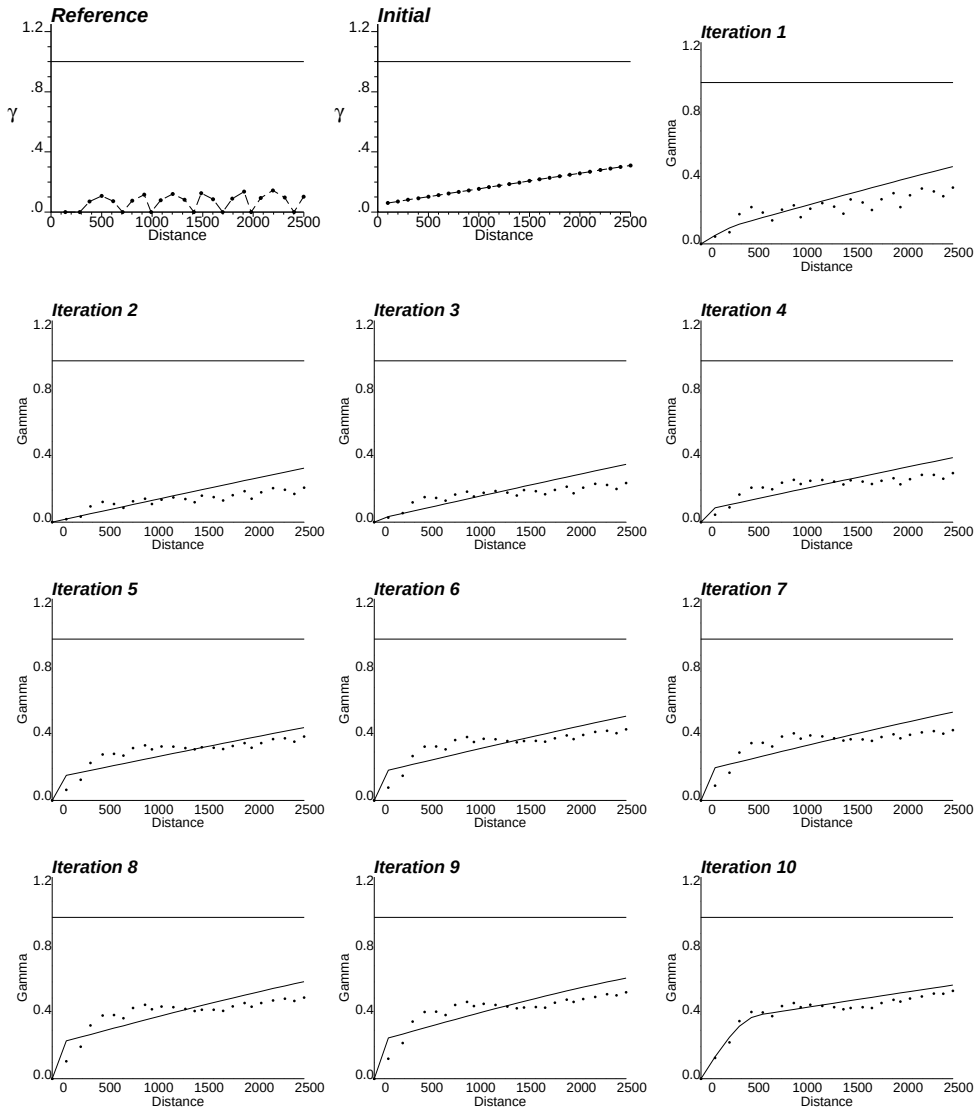


Figure 52: Reference, prior and updated variograms (experimental - dotted line, model - solid line) for $\phi$ at each outer iteration: 8 Well case. (Direction with azimuth 45)

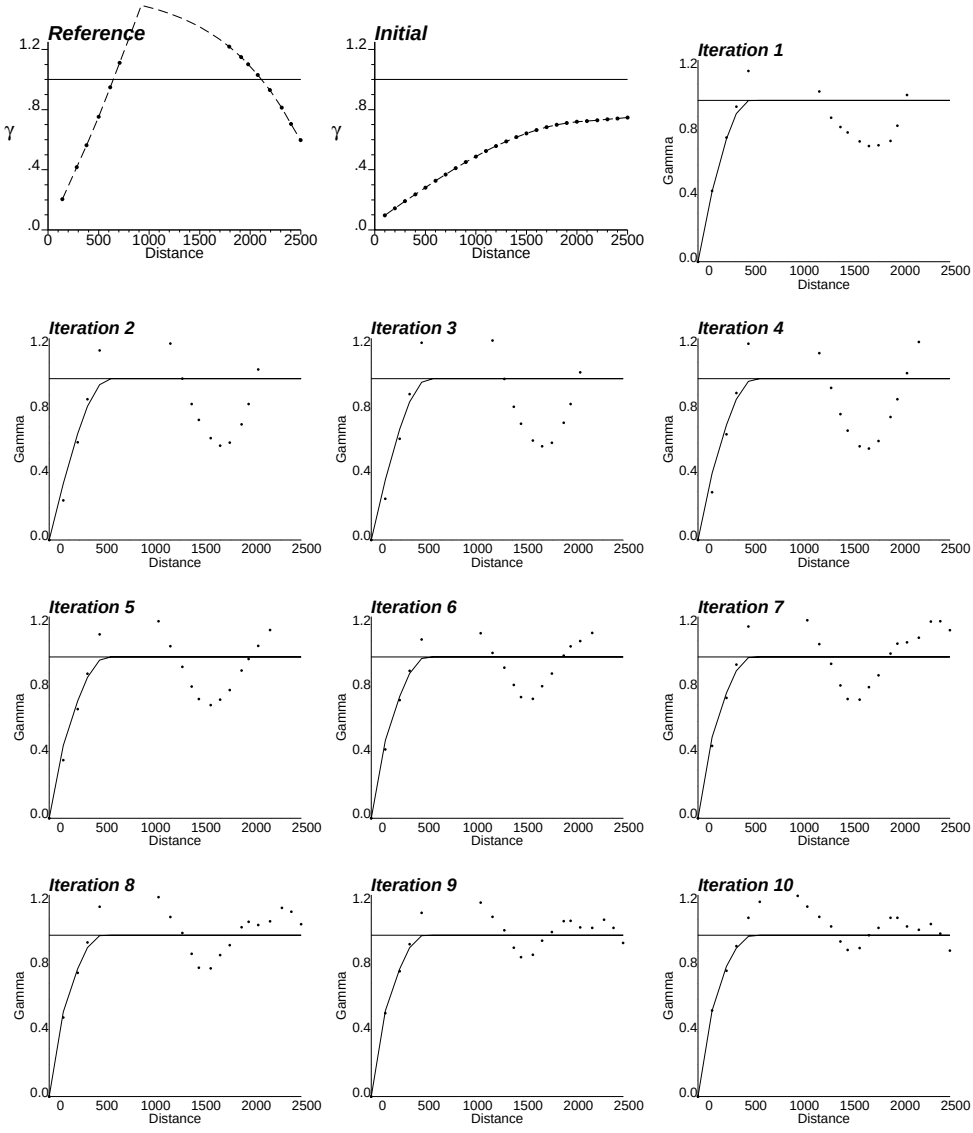


Figure 53: Reference, prior and updated variograms (experimental - dotted line, model - solid line) for $\phi$ at each outer iteration: 8 Well case. (Direction with azimuth 135)

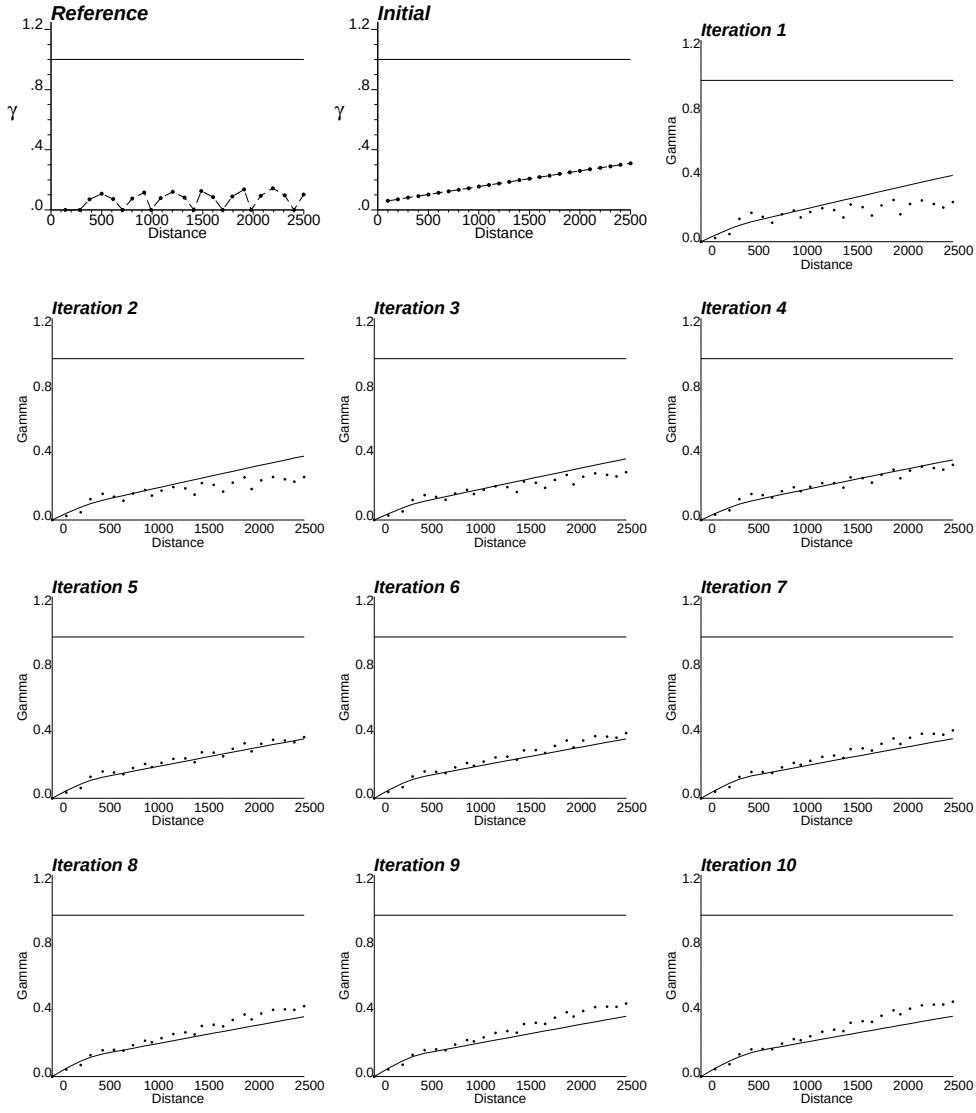


Figure 54: Reference, prior and updated variograms (experimental - dotted line, model - solid line) for $\ln(k)$ at each outer iteration: 8 Well case. (Direction with azimuth 45)

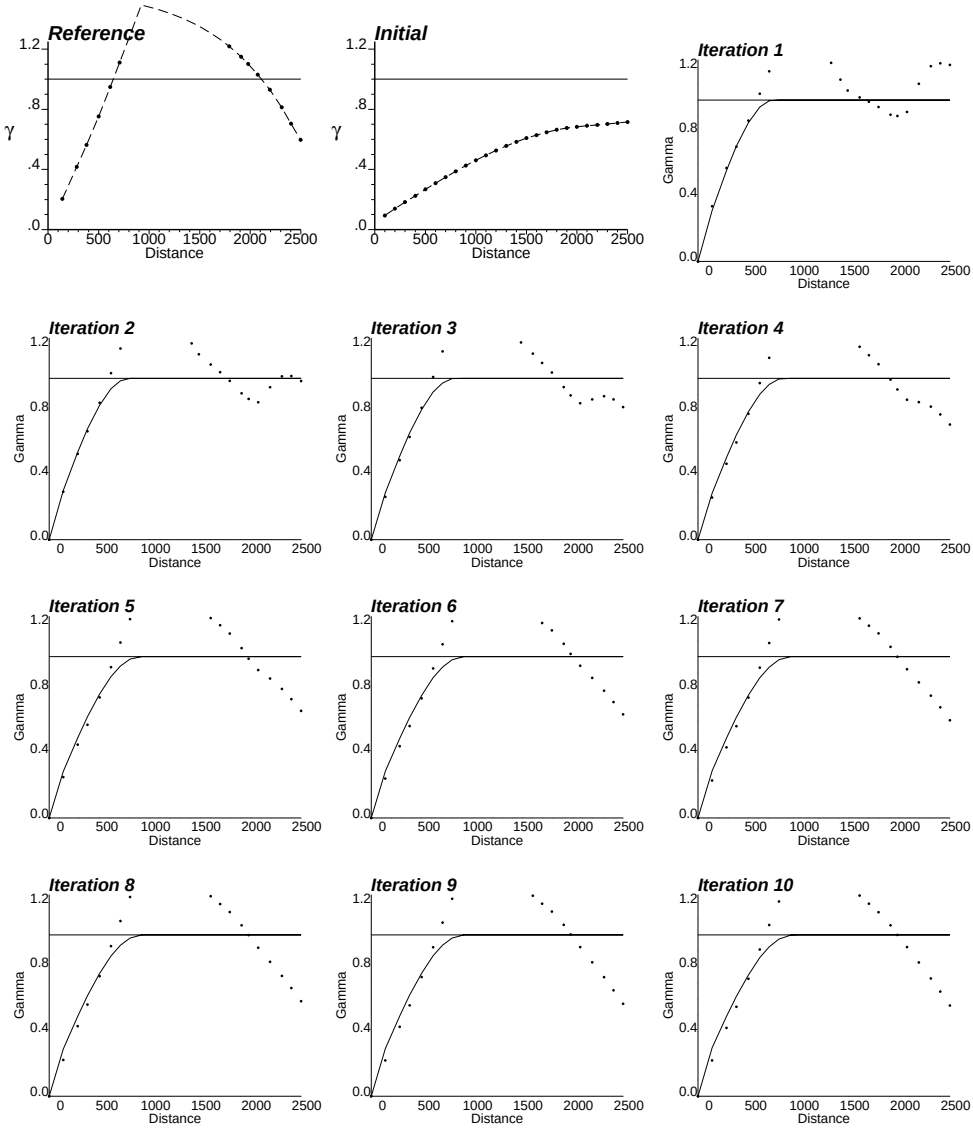


Figure 55: Reference, prior and updated variograms (experimental - dotted line, model - solid line) for $\ln(k)$ at each outer iteration: 8 Well case. (Direction with azimuth 135)

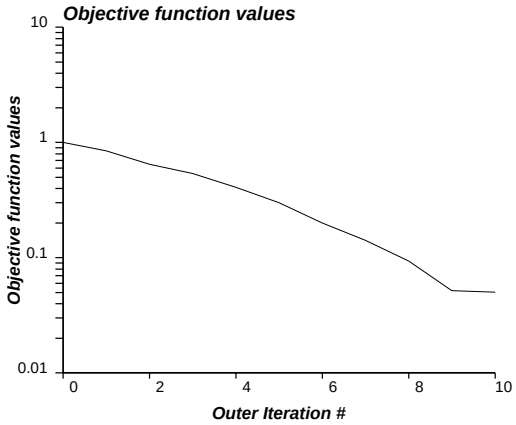


Figure 56: Mismatch norm of data integration at each outer iteration: 8 Well case.

- More production data will improve the inverted variogram models, provided the information is captured in the inversion. A low mismatch value is an index for such evaluation; however, more production data increases the complexity in the nonlinear inverse problem leading to a possible poor match.
- In spite of our objective of getting back the right variogram from production data, we need to start with reasonable variogram models. Gradient-based algorithm requires an initial solution close to the optimal solution.
- The quality of the inverted models depends on the in-built variogram modeling module. It may be possible to further improve on this module by trying different variogram types.
- It might be a good idea to perform the inversion with a prior model having large variogram range values to retrieve the anisotropy information better.
- It also seems that starting with high nugget effect of constant values (no prior structure) works best.

## Some Remarks on Variogram Modeling Module

The in-built automatic variogram modeling module is implemented with an inverse squared distance weighted scheme. Thus, short lag distances are given more weights than the larger distances. Consequently, the updated variogram models do not have good match at large distances.

The perturbation is done on variogram range first, then anisotropy and finally the sill contributions for each nested structure. This cycle is repeated until a convergence with a criterion of threshold number of changes performed. The variograms are modeled to the total sill equal to the variance. No perturbation is done on the variogram type.

Nugget effect is an important parameter for any variogram model. However in a gridded domain, the nugget effect information is limited by the smallest dimension of the grid blocks. A possible solution could be to devise an artificial nugget effect information in the experimental variograms through the use of slopes near the origin (zero lag distance).

## References

[1] Z. A. Reza, X.-H. Wen, and C. V. Deutsch. Simultaneous inversion of porosity and permeability using multiple well production data. In *Report 4*, Edmonton, Canada, March 2002. Center for Computational Geostatistics.